uc3m | Universidad Carlos III de Madrid

Degree in Aerospace Engineering

2017-2018

Bachelor Thesis

Path Controller Implementation for Airborne Wind Energy Systems

Author:

Guillermo Escribano Blázquez

Supervisor:

Gonzalo Sánchez Arriaga

Path Controller Implementation for Airborne Wind Energy Systems

Universidad Carlos III de Madrid

Guillermo Escribano Blázquez

Abstract

The implementation of a path controller to a two-line kite model is presented. Within the first chapter, an introduction to Airborne Wind Energy systems and the discussion of some typical control methods can be found. The following chapter deals with the mathematical model of a two line kite. This model considers a kite-surf size kite that can be controlled via two equal tethers. Some thoughts and explanations on the model are included. Thereafter, an open loop control law capable of allowing figure of eight trajectories is defined. Accordingly, an analytical expression for such figure of eight orbits is presented. Some insight on *Floquet* theory is required in order to properly understand the physics behind periodic orbits. A general purpose predictor-corrector algorithm for periodic orbit propagation determines a set of feasible initial conditions that yield a periodic orbit for a given control law. By means of this tool, it is possible to obtain a periodic orbit applying the control law that has been previously defined. A discussion on such orbit is included, together with its stability analysis. At this point, it is of interest to perform a parametric analysis with the aim of understanding how the stability and the trajectory respond to variations in the control law. Finally the path controller scheme is presented in the form of an optimal control problem. The latter selection was triggered by the failure in implementing a proportional-derivative runtime controller. The results of the project are a deep understanding on the kite sensitivity to variation of tether lengths, i.e. their controls, together with a controller capable of determining optimal control laws for any given desired target path.

Keywords: AWES, Airborne Wind Energy, kite dynamics, two-line kite, optimal control, figure of eight, periodic orbit.

Acknowledgements

I wish to express my sincere thanks to the supervisor of the project G. Sánchez, for the unceasing encouragement, marvellous guidance and invaluable patience, as well as his generous sharing of knowledge and expertise.

I am also grateful to all of the Department faculty members for their willingness to help and support. I am extremely indebted to them for their huge effort and emphasis in transmitting to the students all their wisdom.

I take this opportunity to express my gratitude to my parents. In essence I am the result of the meticulous work that was raising me during 22 years. I am then more proud of them than of myself and will find the way to make them even prouder.

Finally I would also like to express how thankful I am to my girlfriend, from whom I obtained the utmost support. Her inestimable patience and care were crucial pillars for me throughout the project.

List of Figures

List of Tables

Contents

1 Introduction

1.1 Motivation

Climate change is an issue that bothers the whole scientific community so whenever an idea to limit the human impact in this matter arises, it is impossible not to become curious about it. After having attended to an interesting presentation about extracting energy from kites in Mechanics of Flight subject, the choice of my Bachelor's Thesis began to take shape.

On the other hand, Control of Aerospace Systems has always been a subject of interest for me as it requires intuition regarding other areas of aeronautic engineering such as aerodynamics or even structural dynamics. Indeed, the current development of aircraft autopilots, which are "almost" capable of performing a flight without the aid of human interaction, is fascinating for novel engineers like myself.

More importantly, opposed to the typical aerospace applications focused on airplanes or satellites, this project deals with a completely different kind of flying device. The latter fact is thought to improve the student's critical thinking skills, a competence that is becoming more and more demanded by the engineering industry. An individual's adaptive capacity is also of a great importance nowadays, since the trend for working groups is interdisciplinarity. The latter fact implies addressing the previous knowledge and know-how to unprecedented problems or areas of investigation.

1.2 Airborne Wind Energy Systems

A. Cherubini et al. in [8] published a very interesting article on this topic. The current section is essentially a summary of the lessons imparted by A. Cherubini himself during his "Fundamentals of Airborne Wind Energy Systems" course in collaboration with G. Sánchez Arriaga at *Universidad Carlos III de Madrid*. In such course, it was compulsory to deliver a document developing aspects related to the topic. Section 1.2 is an adaptation of this document [5][1].

[1] The author has neither published nor authorized the publication of such document, hence, this shall be the first published article including contents of section 1.2.

1.2.1 General View

As global warming becomes increasingly evident and severe, time for new clean energy production processes has come. Renewable energies might be the only way of reverting climate change and there are currently a lot of efforts in this regard. Apart from hydraulic power, which is a rather cheap source of energy, some renewables still imply significant costs and are not yet self-sustainable in the sense that most of them consume more energy than they provide – an in-depth explanation can be found in Peter Jones' article for isonomia.co.uk[2].

When we think about energy we usually focus just on the electrical one. Such typical mistake does not let us analyze the whole picture. Energy consumed by individuals is not limited to their electrical energy consumption but encloses the energy used to manufacture their clothes, the fuel burnt for their transport, energy invested in growing their food, etc. This means there are a lot more sources of consumption, rendering the assessment of energy distribution a complex task. Following this distribution, it turns out that although renewables are indeed a good choice, there is still much more to be done in order to generate and consume clean energy. Cargo ships and cars yet rely on fossil fuels as an energy source, which implies that although the electrical energy production is shifted towards renewable generation, the overall energy consumption is highly dependent on fossil fuels.

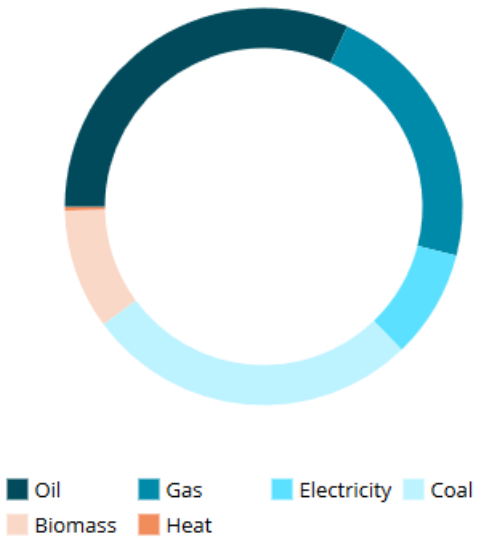

Figure 1.1: 2017 global energy consumption breakdown extracted from enerdata.net[3]

Statement of the previous paragraph can be inferred from figure 1.1, that reveals only the 9% of the global energy consumption comes from electricity. Moreover, they also claim a limited 25% contribution of renewables in electricity production. Photovoltaic

[2] http://www.isonomia.co.uk/?p=5028
[3] https://yearbook.enerdata.net/total-energy/world-consumption-statistics.html

and eolic power generation are currently the most used solutions apart from hydraulic one. Besides the high monetary costs of their facilities, they require a large extension of field in order to deliver a reasonable amount of power, thus limiting their competitiveness. If environmental impact is to be reduced, off-shore farms may be of interest, yielding in turn an important increase in monetary cost. There is not much engineering to be done in order to enhance photovoltaic energy production apart from current researches in material science (i.e. perovskite [7]), yet energy can be extracted from the wind through a wide variety of devices. Wind turbines are huge heavy machines that need a stiff ground foundation in order to stand the high bending moment produced by the wind. If instead of extracting wind energy with a device clamped to the ground a flying one were used, its associated manufacturing and transport costs could be substantially reduced. Indeed an airborne machine might be able to operate at a higher altitude, where wind speed is significantly faster. In the following sections, the energy availability will be discussed, followed by two different approaches for energy extraction and a review of the main actors in the sector.

1.2.2 Power Assessment

Prior to design an airborne system aimed at extraction of wind energy, it is mandatory to perform a power estimation in order to verify the efficiency of such a device. Thus, the inherent energy of the wind may be expressed by use made of the following definition of Wind Power Density:

$$WPD = \frac{1}{2}\rho V^3 \tag{1.1}$$

Measured in $[\frac{W}{m^2}]$, where ρ represents the air density and V is the wind speed.
Recalling that these airborne systems can fly at a higher altitude, and given that wind speed increase with height, it is straightforward to notice that the capabilities of AWES are worth the risk. Notice that despite the fact that air density decreases with altitude, WPD is affected by the third power of the wind speed. The inferred increase in V with height is related with the thickness of the earth's boundary layer (PBL), which extends up to at least 500 m and is responsible for wind deceleration among other phenomena [24]. [4] contains a recent and accurate study on the energy available to AWES in case of fixed or variable altitude operation performed at the west coast of UK, together with an overall study in the the european continent.

After estimating the amount of power inherent to the air, it is time to define a simple model in order to assess the energy that can be extracted using an airborne wind energy system (AWES). This simplified model will consider a kite flying in crosswind, steady state conditions. Under this scenario, the speed of the kite can be much higher than that of the wind – around seven times –, meaning that energy availability is increased by a factor near 300 ($V_k \approx 7 \cdot V \rightarrow WPD_k \approx 7^3 \cdot WPD$). The kite is connected to the ground through a continuously reeled-out tether, thus providing torque to the mechanism employed for extracting energy (Note that the previous fact only applies to

ground generation applications, whereas for onboard generation the tether length is kept constant and energy is extracted by virtue of onboard turbines/devices). Gravity force will be neglected in order to simplify the resulting formula, which yields the following expression for the maximum power output that can be retrieved from an airborne wind energy system [17]:

$$P_{MAX} = \frac{1}{2}\rho V^3 \frac{4}{27} E^2 C_L A \tag{1.2}$$

Where the first three terms correspond to the wind power density (V is wind speed, opposed to kite speed V_k), E is the aerodynamic efficiency of the kite (i.e. lift force over drag force), C_L is the lift coefficient of the kite (defined as $C_L = \frac{Lift}{\frac{1}{2}\rho V_{kite}^2 A}$) and A is the area of the kite.

1.2.3 Power Extraction

Up to now, there has not been given any sense in how is the mechanism of energy extraction in AWE systems, mainly because there are different perspectives from where the problem can be addressed. These are mainly two: on-board and ground generation. In any case it is mandatory to include a tether in the design, either to transmit mechanical power or to drive the generated power – as well as for absolute flow deceleration, which is the source of energy. Designs for each type of system are found to be different. Fabric kites are commonly used for ground-gen systems while composite drones are the main drivers of fly-gen ones.

- **Ground-gen AWES:** In this design power is extracted by utilizing the tension on the tether(s) of the kite to rotate a ground generator. The optimal flight path of the kite are lying eights along the wind window[4] in which the cable is reeled-out in order to move the ground electrical generator. Energy is injected into the system during a second reel-in phase in which the flying wing is either depowered or in a flagged state, thus leading to a duty cycle. There are thoughts on implementing a carousel type ground generator powered by numerous kites with the aim of enhancing energy extraction. Ground-gen kite designs can also be extrapolated to traction of cargo ships. Some players have claimed a reduction of up to 25% of fuel consumption in their designs, however, a 10% reduction would be a more realistic figure. Difficulties in take-off and landing phases arise due to flexibility of kites, preventing fully automated operation. Losses in mechanical transmission at the tether-powered ground generator are to be compared to power efficiency of airborne energy production devices in fly-gen systems.
- **Fly-gen AWES:** Another way of power extraction contemplates the possibility of implementing on-board wind turbines in order to directly decelerate the relative flow to obtain power. No duty cycle is required now since circular trajectories

[4] The wind window is defined as the plane perpendicular to the wind velocity.

are a good trade-off between power optimization and simplicity, facilitating the implementation of multiple-kite carousel-type designs that by sharing a cable segment, allow for a better efficiency. This leads to injection of energy only at the take-off stage, which can indeed be achieved by utilizing the on-board generators as thrust providers. Then the tether is used both for enabling power extraction and driving the electric current generated so to be further distributed on ground. Stationary balloon-like stations have also been studied but their limited output energy (referred to energy availability) compared to that of flying ones may relegate them to second place in the future. As it was previously inferred, rigid wing drones similar to sail planes are currently the main aircraft design type due to their high lift and easier implementation of automatic controls. They present difficulties in horizontal landing due to cable constraints, whose current solution is to detach the cable at the final approach stage. There is a scalability problem with the cable meaning that implementation for MW-order designs may require the use of advanced materials for electric conduction and/or cable reinforcement, greatly increasing manufacturing costs or electrical resistance through the tether.

1.2.4 Main Players

- **TU Delft**[5]**:** It is one of the leading universities in wind power generation research. Currently working with leading edge inflatable (LEI) kites, their ground-gen design is able to deliver up to 20 kW of electrical power with an average of around 4 kW. It features a single tether design with control pod. They also have some prototype design that is meant to deliver a peak of 100 kW.
- **Skysails Marine**[6]**:** Company aimed at kite designs for cargo ship traction. Their prototypes are based on ram air kites (similar to paragliding ones) with fully automated control system via a control pod. They are the ones that claim fuel savings of up to 25%. Launch and recovery of the device is favored due to offshore wind availability, which makes the implementation of fabric kites more appropriate than in land areas.
- **KiteGen**[7]**:** Its main design features a semi-rigid wing kite aimed at ground power generation. Made of composite materials it has the dimensions of a large airliner wing and is composed by 9 CFRP segments hinged with flexible joints. Notice that this kind of design has some disadvantages mainly in the landing phase due to its fragility, meaning that operation might only be possible at high stable ground wind speeds.
- **Twingtec**[8]**:** Swiss company focused on drone designs with on-board take-off motors and ground-gen systems. It features a totally automated operation thanks to

[5] http://www.kitepower.eu/
[6] https://www.skysails.info/en/
[7] http://www.kitegen.com/en/2014/09/12/kitegen-power-wing/
[8] http://twingtec.ch/

these on-board motors and its current design has a rated power of 100 kW with 15 m wing span. Such design (TT100) is presented as a containerized device that can be easily installed in remote areas.

- **Joby Energy**[9]**:** Bi-plane aircraft with on-board generators aimed at high lift generation and featuring vertical take-off and landing. It has to face several structural problems related to multi-plane designs, in which drag is a main concern.
- **Skypull**[10]**:** Swiss company also focused on multi-plane kites but based on ground generation. In this case a low aspect ratio wing type with onboard motors for take-off and landing is implemented.
- **Altaeros**[11]**:** Autonomous tethered aerostat designed to operate around 600 m above the ground. It consists in a lightweight wind turbine lifted by a balloon. One of its main problems consists in the blowdown angle caused by drag force.
- **Sky Windpower**[12]**:** Self-lifting multi-rotor devices similar to the usual quadcopter drones are intended to be used as fly-gen systems. They are based on the idea of the Australian engineer Bryan W. Roberts of a "Flying Electric Generator" (FEG) or "rotorcraft".
- **Makani Power**[13]**:** Arguably developing the most advanced prototypes for wind harness, it focuses on drones equipped with on-board generators that can be used for take-off and landing purposes. This California-based company was acquired by Google in 2013. Starting with soft kites in 2006, they moved to rigid aerodynamic wings and their latest working prototype (M600) should be able to generate 600 kW of maximum rated power with a wingspan of 26 m. Makani's goal is to manufacture a kite capable of producing a rated power of 5 MW, whose current design stage claims a full rated power wind speed of 9 m/s at an operational altitude range of 350-650 m featuring a 65 m wingspan and 8 on-board brushless motors.

1.3 Typical Control Solutions

1.3.1 PID Controller

Due to its simplicity, it is usually the controller type to be implemented as a first approximation. It inherits the error in a given state variable (i.e. the difference between the desired value and the actual one) and translates this error in a control actuation. Tuning Proportional-Integral-Derivative controllers essentially consists in

[9] http://www.jobyenergy.com/img/media/joby_energy_tech.pdf
[10] https://www.skypull.technology/solution
[11] http://www.altaeros.com/energy.html
[12] http://www.skywindpower.com/
[13] https://x.company/makani/technology/

varying its three constants until the response of the system fulfills the requirements of the user. These three constants that govern its behavior are defined as:

- **Proportional:** Direct relation between the error and the control actuation.
- **Integral:** The controller performs a numerical integration of the error in order to account for historical data. This feature ensures that the final value of the variable to be controlled exactly matches the desired one, i.e. it eliminates the steady state error. However, it may produce small oscillations in the response if not properly tuned.
- **Derivative:** Numerical derivation of the signal is also carried out to enhance the speed of the response. By selecting a proper derivative constant, the time it takes for the variable or signal to reach the neighborhood of its desired value can be greatly minimized.

PID controllers are broadly used in linear systems thanks to their fair responsiveness and high reliability. Indeed, they can be extrapolated to non-linear models through prior implementation of Non-Linear Dynamic Inversion (see: [15] and citations "[33]-[34]" inside).

1.3.2 Model Predictive Control

Model Predictive Control relies on the ability of the model to propagate the current dynamics up to a given time horizon. This way, it is possible to determine the set of control actuations that best suit the desired evolution of the system. Chapter 20 in [23] contains an in-depth explanation on how to implement the MPC technique. Recall that it is typically used in Multiple-Input Multiple-Output linear systems with control saturation in which a cost function is to be minimized.

Despite the lack of linearity present in the current model, finite horizon propagation might be of aid in targeting a predefined trajectory. Therefore, if linearization of the dynamics is accurate enough in the surroundings of the target trajectory, this control technique will definitely be considered. Note that dynamics of non-linear models may require a significant computational cost, thus precluding any MPC implementation from continuous, real time applications.

1.3.3 Non-Linear Dynamic Inversion

The main idea of NDI is to find some "virtual control input" to which the system responds in a linear manner [6]. This input is transformed into a former control actuation afterwards. In order to apply such method directly the system must be written in "companion form", otherwise input-output linearization shall be performed.

The "virtual control input" is defined as:

$$v = a(\mathbf{x}) \cdot u + b(\mathbf{x}) \tag{1.3}$$

Where $a(\mathbf{x})$ and $b(\mathbf{x})$ are retrieved when a linear relation between the input u and the output y of the system is found, that is:

$$y^{(k)} = a(\mathbf{x}) \cdot u + b(\mathbf{x}) \tag{1.4}$$

In which $y^{(k)}$ represents the k-th derivative of the output with respect to time. Finally, by selecting $v = y^{(k)}$ the system would be linearized based on its output.

The relative degree **k** of the system is always $k \leq n$, where **n** is the number of state variables (i.e. the order of the system). In case $k < n$ some dynamics would not be "observed" by input-output linearization, meaning that this scheme would not take any control action over them. The latter fact strictly requires these "internal dynamics" to be stable, otherwise the system will not be controllable under NDI technique. An application can be found in [6], while the academic-oriented notes were extracted from a TU Delft course[14].

1.3.4 Dynamic Backstepping Control

The backstepping method consists in dividing the whole system model into different subsystems. All these subsystems will be connected in series through a set of "virtual controls". Subsequently a Control Lyapunov Function (CLF) will be used as control law at each subsystem with the aim of mapping each intermediate state vector to its corresponding "virtual control".

Dynamic backstepping is an evolution of the typical backstepping technique aimed at general pure-feedback systems, overlapping the strict-feedback oriented regular method. This is achieved by propagating the dynamics of the "virtual controls" (i.e. as if they were state variables) through each interconnection between subsystems. Therefore, an additional CLF has to be implemented at each stage. S. Zhang and W.-q. Qian in [29] thoroughly discuss such technique and present a tracking application with strong results. Nevertheless, for higher degrees of complexity the control functions might require more sophisticated solutions such as neural-network adaptive control [28].

[14] http://www.aerostudents.com/courses/advanced-flight-control/nonlinearDynamicInversion.pdf

1.4 Objectives

This project essentially aims at the implementation of a tracking-type controller into the non-dimensionalized two-line kite model developed by G. Sánchez et al. in [26], which follows a Lagrangian formulation. In non-dimensional models, scaling the system only affects the dynamics if the aerodynamic characteristics (as defined in [9]) are altered. The reader should note the convenience of this feature since scaling is a major concern in the renewable energy industry, especially for novel technologies such as Airborne Wind Energy [10].

The most typical trajectory followed by acrobatic kites is a figure-of-eight (hereafter **FOE**). Energy extraction through AWES requires periodic orbits, rendering FOEs the best candidates for two-line configurations as they avoid entangled tethers. The main objectives of the current project are listed below:

- Verify the system is able to perform a periodic FOE trajectory and explore a family of periodic orbits.
- Implement the MATLAB model into SIMULINK, since the latter environment is more suitable for controller implementation.
- Implement a path controller capable of following a target trajectory.
- Explore the applicability of the path controller, i.e. the range of target FOEs it is able to track.
- Develop intuition regarding the model through variations in the environment and target path.

This project lies within the AWES line of research of the *Bioengineering and Aerospace Engineering Department* at *Universidad Carlos III de Madrid*. A reference document can be found in the Master Thesis developed by A. J. Otero Ramírez [21]. The latter project focuses on the physical implementation, whereas the current one is based on a simulation environment control approach. In the end, both branches are expected to merge in a fully functional control system implemented in a kite-surf wing. The work presented in [15] and [11] falls under the same line of research, rendering them good references for the sake of comparison. Indeed, Manuel Soler et al.[15] in [25] developed a controller in the form of an optimal control problem. It is important to note that despite they are all based on two-line kite models, such models feature an additional "power" tether used to control the angle of attack of the kite, i.e. they feature de-powering capabilities. This lack of control present in the system was not considered important at first but may have severe implications in the overall system controllability.

[15]Staff of *Dynamics and Control of Aerospace Systems Group* of the *Bioengineering and Aerospace Engineering Department* at *Universidad Carlos III de Madrid*.

2 | Two-Line Kite Model

2.1 Description of the Model

The numerical model corresponds to KiteAcrobat under LAgrangian Kite SimulAtors[1] (LAKSA) project [22], developed by Gonzalo Sánchez Arriaga and Alejandro Pastor Rodríguez among others. This system consists in an acrobatic foil rigid kite attached to a point in the ground through two identical tethers. The length of each tether can be controlled separately and they are connected to the kite at either side of the latter, as illustrated in figure 2.1. The current three-dimensional rigid body problem features a reduction of 2 DOFs over the typical 6 DOFs of the free rigid body problem, caused by the restrictions imposed by both tethers. However, if one is eager to use the typical Newtonian (or Classical) mechanics formulation, the aforementioned constraint forces must be retrieved prior to the full resolution of the problem. This is the main reason why Sánchez Arriaga et al. opted for a different formulation approach. Such approach is merely based on Lagrangian formulation, in which determination of holonomic constraints like those imposed by the tethers can be avoided through a proper selection of the coordinate system. A further insight on these matters can be found in [13]. Apart from the assumption of the kite acting as a rigid body (which entails some limitations in terms of angle of attack and sideslip angle), both tethers are considered inelastic. This fact implies that their length is independent of the tension that is acting on them, thus not affecting the kite motion. One last assumption, albeit not valid for a detailed model, considers the tether elements massless and one-dimensional so that neither gravity nor aerodynamic forces can deform their straight shape. Therefore both tethers will act as rigid rods that can only support positive tension. Note that mechanical waves traveling through them will be longitudinal as a result of control actuations, so slow dynamics near to the model time scale such as transversal waves are improbable. Such hypothesis is in accordance with the intended simplicity of the model, mainly focused in developing intuition for two-line kite dynamics. A flexible tether, single-line kite model was implemented by A. Pastor et al. in [19].

[1] https://github.com/apastor3/laksa

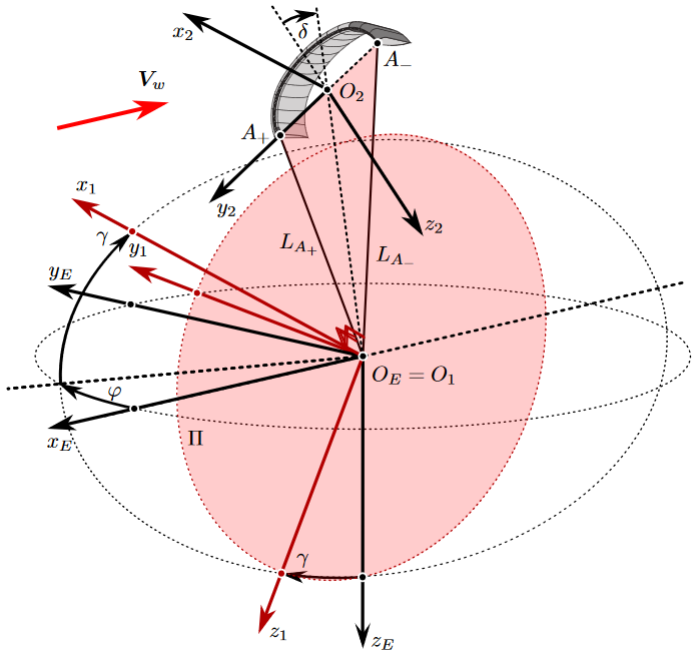

Figure 2.1: Detailed sketch of the kite system extracted from [26].

The definition of the first two degrees of freedom is presented in 2.1, corresponding to the angles defined as φ and γ. The former rotation is performed about the z-axis of the earth fixed reference frame, identified by the subindex $_E$, defining the y-axis of a new frame of reference S_1 centered in $O_1 \equiv O_E$. The latter rotation (given by the angle γ) occurs about the y_1-axis, thus fully determining the reference frame S_1 through its x and z-axes. Next rotation η is performed about the x_1-axis and it yields the vector components of the frame S_2. This new reference frame is centered in O_2, positioned midway between the segment that joins both tether attachments at the kite, A_+ and A_-. Scheme on the right of figure 2.2 shows the rationale of the last rotation θ, usually referred to as the elevation or pitch angle, which is closely related to the angle of attack of the body[2]. It translates the O_2 frame to the typical body-fixed reference frame, located at the center of gravity of the kite, G. The use of such frame of reference has some well-known implications mainly in the inertia tensor of the system, which now does not depend on the position nor on the attitude of the body - it is therefore constant. Indeed, by selecting the proper body axes, referred to as principal axes, the inertia tensor becomes a diagonal matrix, greatly simplifying the the resulting equations of motion and the computational time required to solve them. This was indeed the choice made in [26] for the current model.

[2] Typically, the elevation angle is defined with respect to the earth horizontal plane. Note that in this case, θ is a sort of local elevation angle that infers the attitude of the kite body with respect to the tether attachments $A_\pm$.

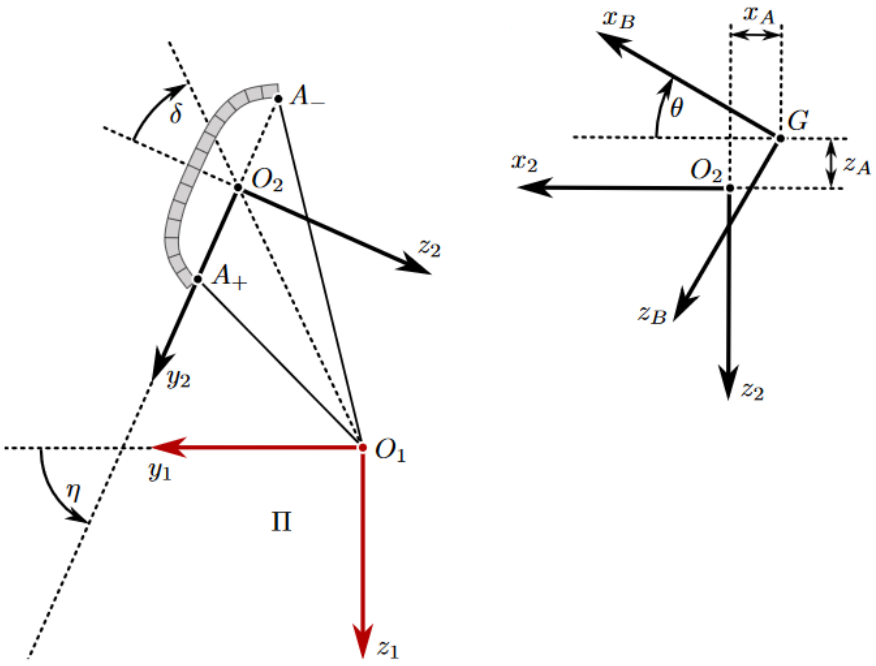

Figure 2.2: Definition of η and θ borrowed from [26].

After introducing the state variables of the system it is mandatory to define the controls that will be used throughout the study. These controls obviously correspond to the length of each tether, but during the development of the model two different definitions arose as the most "natural" ones - essentially because they imply important simplifications in the equations of motion. One of them has been already included in both figures 2.1 and 2.2 (on the left sketch) and is denoted by δ. It is related to the difference between the length of both tethers (antisymmetric deflection) and is defined as the angle formed between the z_2-axis and the line that joins O_1 and O_2. Its mathematical expression reads as follows:

$$\delta = \arcsin\left[\frac{\ell_{A_+}^2 - \ell_{A_-}^2}{4\ell y_A}\right] \tag{2.1}$$

The other control variable is explicitly included in equation 2.1 above and is denoted by the letter ℓ. Symmetric deflection will be then indicated by ℓ, which can be thought of as a mean length of both tethers.

$$\ell = \sqrt{\frac{1}{2}(\ell_{A_+}^2 + \ell_{A_-}^2 - 2y_A^2)} \tag{2.2}$$

There are three important geometric parameters that relate the length of each tether to the aforementioned control variables, and they can be visualized in figure 2.3.

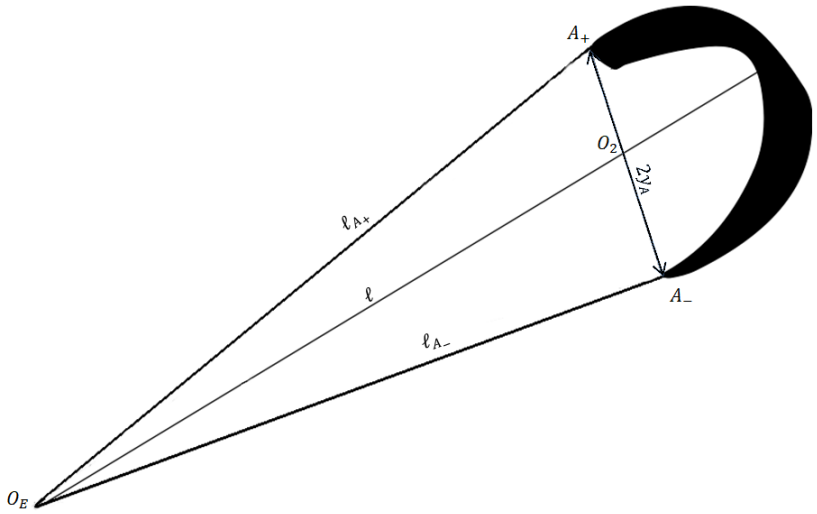

Figure 2.3: Sketch of tether-related geometric parameters.

Whilst $\ell_{A_\pm}$ can be both varied, $2y_A$ is fixed for a given kite geometry if the kite is assumed to be undeformable.

Once the control and state variables are fully determined, it is possible to write the equations of motion of the system as follows [3]:

$$\frac{d\mathbf{x_s}}{d\tau} = \mathbf{f}(\mathbf{x_s}, \mathbf{x_c}, \dot{\mathbf{x}}_\mathbf{c}, \ddot{\mathbf{x}}_\mathbf{c}) \tag{2.3}$$

Where the state and control vectors are defined as:

$$\mathbf{x_s} = \begin{pmatrix} \varphi & \gamma & \eta & \theta & \dot{\varphi} & \dot{\gamma} & \dot{\eta} & \dot{\theta} \end{pmatrix} \tag{2.4}$$

$$\mathbf{x_c} = \begin{pmatrix} \ell & \delta \end{pmatrix}, \tag{2.5}$$

N.B.: At first glance, the system could be characterized as non-autonomous since its dynamics are dependant on some arbitrary control inputs. However, once a control law has been defined the system does no longer have any degree of freedom, so it automatically becomes autonomous.

There is some important clarification about the model that is related with equation 2.3. It can be noted that the derivative of $\bar{x}_s$ is made with respect to τ, which is clearly not the time. This is due to the whole model being non-dimensional, so that for example

[3] For a detailed description on how to obtain the equations of motion and their full expressions please refer to [26].

$\tau = t\sqrt{g/L_0}$ and $\ell_{A_\pm} = L_{A_\pm}/L_0$, with L_0 being the initial length of one of the tethers. Please note that $\dot{x} = dx/d\tau$ according to the definition of the non-dimensional time.

Even though the whole model is based on non-dimensional parameters, it is of interest to yield some results with dimensions so as to have a better understanding of them. For this particular purpose, the following dimensional parameters corresponding to a typical kitesurf wing will be used.

Table 2.1 Geometric and physical parameters of the model

Symbol	**Definition**	**Value**
c	Mean chord	1.5 m
b	Span	5.8 m
A	Surface	14.4 m^2
m	Kite's mass	4 kg
Ix	Moment of inertia about x	21.1 kg m^2
Iy	Moment of inertia about y	4.66 kg m^2
Iz	Moment of inertia about z	18 kg m^2
g	Gravity acceleration	9.81 m/s^2
ρ	Air density	1.225 kg/m^3
V_w	Wind velocity	7 m/s
L_0	Main reference length	200 m

The motion of the kite strongly depends on its aerodynamic characteristics, represented by the following non-dimensional coefficients according to Etkin's [9] definitions and model. Aerodynamic limits on maximum angle of attack and maximum sideslip angle due to kite stall or deformation are also included in table 2.2 below.

Table 2.2 Model Aerodynamic Parameters

Force Coefficients		**Torque Coefficients**		**Limits**	
Symbol	**Value**	**Symbol**	**Value**	**Symbol**	**Value**
C_{x_0}	-0.065	C_{l_β} [4]	-0.1	α_{stall}	25^o
C_{x_α}	0.18	C_{l_p}	-0.15	β_{max}	15^o
C_{y_β}	-1.57	C_{m_0}	0.13		
C_{z_0}	0.116	C_{m_α}	-0.76		
C_{z_α}	-2.97	C_{m_q}	-0.17		
		C_{n_β}	-0.027		
		C_{n_r}	-0.002		

2.2 Analytical Control Law

In this section, a feasible analytical control law will be presented and discussed. Such control law shall drive the kite to follow some periodic figure-of-eight. The aspect of the trajectory is not of a great importance since direct, open-loop control is merely a trial and error procedure.

The control schedule must be periodic and, according to the dynamical system, bounded up to the second derivative. This can be observed in the simple expression of eq. 2.3, where the derivatives of the state variables seem to be affected by both the first and second derivatives of the control vector. Indeed, the control variables δ and ℓ have a very strong influence in the position of the center of gravity of the kite, not to mention the high impact δ has in its attitude. Following with the study of the controls, one may notice that variations in ℓ could hinder the solution to the problem. This means that the only control to be utilized will be δ and its acceleration shall at least be bounded in order for the model to accurately represent the dynamics - jumps in $\dot{\delta}$ would disrupt the continuity of the system. Although the initial conditions are a crucial element of the control schedule, their discussion will be relegated to a later section which is purely dedicated to periodic orbit theory.

The selected design is based on a sinusoidal function delayed at its maximum and minimum values. That is, two invariant time steps at maximum and minimum control actuation are welded together by a cosine segment (either rising or falling). The mathematical expression for such a control sequence read as follows:

$$\delta(\tau) = \begin{cases} \delta_{max} & \tau \leq \tau_1 \\ \delta_{max}[\cos(\pi \frac{\tau - \tau_1}{\tau_2})] & \tau_1 \leq \tau \leq \tau_1 + \tau_2 \\ -\delta_{max} & \tau_1 + \tau_2 \leq \tau \leq 2\tau_1 + \tau_2 \\ -\delta_{max}[\cos(\pi \frac{\tau - 2\tau_1 - \tau_2}{\tau_2})] & 2\tau_1 + \tau_2 \leq \tau \leq 2\tau_1 + 2\tau_2 \end{cases} \tag{2.6}$$

Three parameters define the control schedule then, namely τ_1, τ_2 and $|\delta_{max}|$, defined in figure 2.4 below. It can be shown that the first derivative of 2.6 with respect to τ is continuous because it is basically a sine. The second derivative, however, features some jumps at the beginning and the end of each transition between δ_{max} and δ_{min}. These facts can be observed in figure 2.5, which contains the evolution of both $\dot{\delta}$ and $\ddot{\delta}$ for the same parameters selected in figure 2.4.

[4] This parameter plays an important role in the kite motion. [26] contains an in-depth study on how its value affects the stability of the kite configuration.

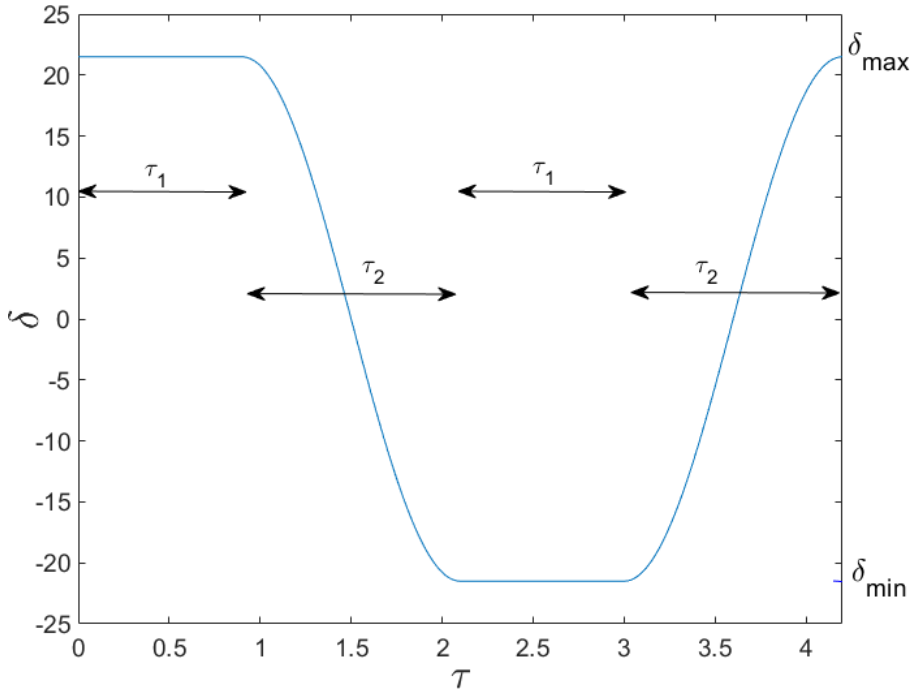

Figure 2.4: Variation of δ during a full period.

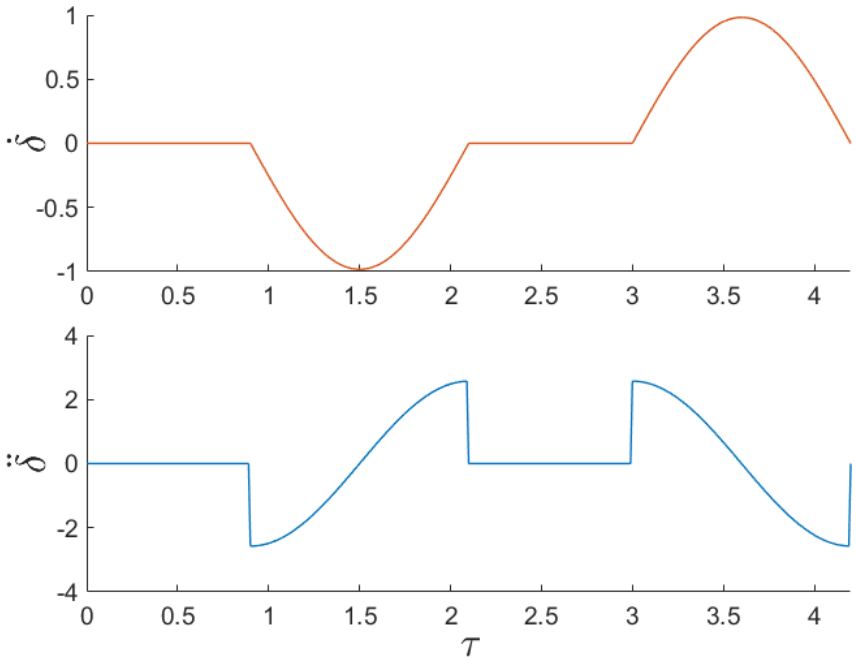

Figure 2.5: First and second derivatives of 2.6.

2.3 Analytical Trajectory

Lemniscates, a special case of Lissajous' figures, are very good candidates to define a broad family of figure-of-eight shapes, as C. Jehle infers in [15]. Indeed, these analytic expressions naturally arise when an infinity-symbol like trajectory wants to be defined - even in the case of novel engineers. Figure 2.6 shows the definition of two angles, χ and λ. The former is the result of a rotation around the z_E axis so the center of gravity G is contained in the plane formed by the x_1 and z_1 axes. The latter, λ, corresponds to the magnitude of the rotation about y_1 that would align a new x_2 axis with the segment $\overline{O_E G}$. Please note S_2 reference frame corresponding to last rotation λ is not included in figure 2.6 for the sake of simplicity.

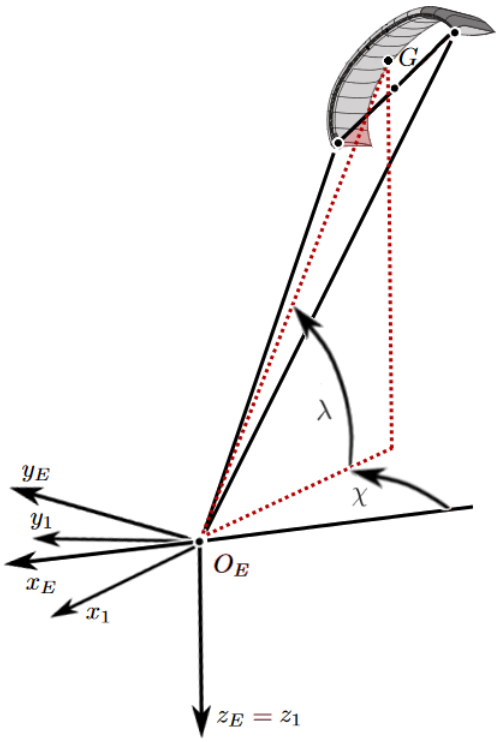

Figure 2.6: Adaptation of figure 2.1 (which was extracted from [26]) to illustrate the definition of χ and λ.

$$\lambda(u) = \lambda_0 \sin(2u) + \lambda_1 \qquad (2.7) \qquad\qquad \chi(u) = \chi_0 \sin(u) \qquad (2.8)$$

Considering the expressions for λ and χ given by 2.7 and 2.8 as a function of some parameter u, it is possible to determine a family of analytical FOE trajectories. The height, width and mean altitude of the trajectory are given by λ_0, χ_0 and λ_1 respectively. An example trajectory in the λ-χ plane is presented in figure 2.7.

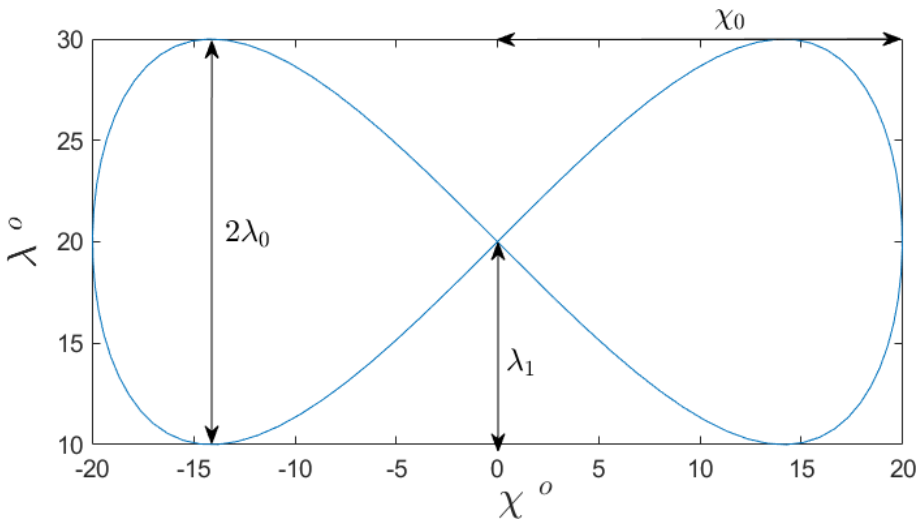

Figure 2.7: Analytical trajectory for $u \in [0, 2\pi]$ in the λ-χ plane.

Two relations are still needed to adapt this analytical FOE to the model. The evolution of the variables that define the trajectory are a function of u, whose relation to the model variables read as follows:

$$u = \frac{1}{2\pi}\frac{s(\tau)}{s_f} = \frac{1}{2\pi}\frac{\int_0^\tau ||\dot{\mathbf{x}}_{\mathbf{cg}}||d\tau}{\int_0^T ||\dot{\mathbf{x}}_{\mathbf{cg}}||d\tau} \tag{2.9}$$

Where s is the arc-length of the trajectory and T is the period of the periodic orbit. Then it is possible to retrieve the target or analytical position of the center of mass with respect to the earth reference frame S_E through direct application of the expression below:

$$\mathbf{x}^*_{\mathbf{cg}} = ||\mathbf{x}_{\mathbf{cg}}|| \begin{bmatrix} -cos(\lambda)cos(\chi) \\ cos(\lambda)sin(\chi) \\ -sin(\lambda) \end{bmatrix} \tag{2.10}$$

Two key aspects should be remarked with regard to the determination of u:

- It is necessary to know the runtime magnitude of the position and velocity of the center of mass of the kite with respect to the earth frame ($||\mathbf{x}_{\mathbf{cg}}||$ and $||\dot{\mathbf{x}}_{\mathbf{cg}}||$). In fact, the magnitude of the velocity must be known for the whole trajectory. This is usually not feasible in real time applications so the definition of u in equation 2.9 is relegated for an optimal control implementation.
- In case the controller to be implemented is real time oriented, it may be possible to obtain the value of u that minimizes the distance between the current position of the center of mass $\mathbf{x}_{\mathbf{cg}}$ and the analytical or target one $\mathbf{x}^*_{\mathbf{cg}}$.

3 | Natural Periodic Orbits

3.1 Periodic Orbits Theory

A periodic solution to a system of equations with minimum period T is such that $\mathbf{x}(t) = \mathbf{x}(t+T)$ and indeed, $\mathbf{x}(t) \neq \mathbf{x}(t+\tau)$ for all $0 < \tau < T$. This implies they are closed trajectories in the state space in the sense that the initial conditions are reached cyclically after a time span given by its period. Periodic solutions can seldom be determined analytically. Numerical methods such as *shooting*, *spectral* or *finite differences* are the most extended. A relatively simple procedure consists in using a *first recurrence* or *Poincaré* map [2]. The first step is to define a hypersurface transversal to the trajectory at some initial point:

$$\mathbf{n}(\mathbf{x}) \cdot \mathbf{f}(\mathbf{x}, t) \neq 0 \tag{3.1}$$

Where $\mathbf{n}$ represents the hypersurface normal and $\mathbf{f}(\mathbf{x}, t) = \dfrac{d\mathbf{x}}{dt}$. The dynamics of the system are then propagated until the trajectory crosses the *first recurrence* map again. In case this last intersection does not coincide with the proposed initial condition (i.e. $\mathbf{x}_0 \neq \mathbf{x}(T)$), the latter needs to be corrected. The logical step after obtaining a periodic solution is to determine its stability. *Floquet* theory is the means by which the stability of such solutions can be addressed. As usual, the idea is to perturb the system in the neighborhood of the periodic orbit so that the resulting state would be:

$$\mathbf{x}(t) = \mathbf{x}_p(t) + \boldsymbol{\xi}(t) \tag{3.2}$$

Being $\mathbf{x}_p(t)$ the periodic solution and $\xi(t)$ a small perturbation.

Given that $\xi(t)$ is sufficiently small, it is possible to linearize the motion along the whole trajectory making use of a Taylor expansion. If one retains only the first order terms what remains is the Jacobian of the system evaluated at a given time stamp t^*[1], that is:

[1] For numerical analysis, a collection of Jacobian matrices must be retrieved in numerous points at the discretion of the user. Nevertheless, this collection must provide a proper interpolation grid to ensure the validity of the approximation.

$$\bar{\bar{J}}_{ij}(t^*) = \left.\frac{\partial \mathbf{f}_i(\mathbf{x}, t)}{\partial \mathbf{x}_j}\right|_{\mathbf{x}_p(t^*)} \tag{3.3}$$

For $i = 1, ..., m$ and $j = 1, ..., n$, where m and n are the sizes of $\mathbf{f}$ and $\mathbf{x}$ respectively.

Now the linearized system can be written as follows:

$$\frac{d\boldsymbol{\xi}}{dt} = \bar{\bar{J}}(t) \cdot \boldsymbol{\xi} \tag{3.4}$$

The system described by 3.4 has n linearly independent solutions. These solutions can be readily obtained by integrating equation 3.4 n times, each time with a different initial condition such that $\xi_i(0)$ equals the *i-th* row of the $n \times n$ identity matrix $\bar{\bar{I}}_{n\times n}$. If all the integrations are performed from $t = 0$ to $t = T$ using the above set of initial conditions, it is very simple to construct the *Monodromy* matrix[2]:

$$\bar{\bar{M}} = \begin{bmatrix} \boldsymbol{\xi_1}(T) & \cdots & \boldsymbol{\xi_n}(T) \end{bmatrix} \tag{3.5}$$

Such matrix can be defined as a map or transformation that yields the position of a point in the state space at regular intervals of time T (i.e. $\mathbf{y}(T) = \bar{\bar{M}} \cdot \mathbf{y}(0)$). The eigenvalues of the *Monodromy* matrix are called *Floquet multipliers* and determine the convergence or divergence of the response along their associated eigendirection. This implies that for a periodic solution to be stable, all its *Floquet multipliers* must have a magnitude strictly lower than one. There are particular cases in which unitary eigenvalues can be obtained without compromising the stability of the periodic solution. That is the case of autonomous systems, defined as those in which the laws that govern the motion of the state variables only depend on their position regardless of the time. Since they may feature one unitary *Floquet multiplier*, perturbations in the tangential direction to the orbit will remain constant. On the other hand, if the system were non-autonomous the orbit would be characterized as non-hyperbolic, and the study of its stability would require a non-linear analysis so as to determine the implications of this unitary eigenvalue.

[2] [13] contains an in-depth explanation on these matters, covering educational aspects that are not relevant for the present work.

3.2 Predictor-Corrector Algorithm

Hereafter, the predictor-corrector algorithm used to retrieve periodic solutions will be presented. This kind of solver in the form of a MATLAB routine was provided by the supervisor of the present work, based on the numerical algorithm presented by M. Lara and J. Peláez in [18]. Their article is focused on 3 degrees of freedom conservative systems, providing as example the typical Restricted Three-Body Problem. G. Sánchez approach considers a broader application that is valid for non-autonomous systems as the current one. Since non-autonomous systems do not feature trivial solutions coming from tangential deviations, there is no need to reduce the order of the system and the algorithm can be readily applied to it without any modification.

The MATLAB routine inherits the following inputs:

- The equations of motion of the system by means of a MATLAB function.
- A guess for the initial conditions.
- The period of the periodic orbit, given by that of the control schedule in this case.
- Some tolerance for the error between the initial and final state, below which convergence is assumed.
- Absolute and relative tolerances for the ODE solver.
- The numerical step of the Jacobian, used in the linearization of the system.
- The maximum number of iterations, after which the execution is finished.

It then outputs:

- The corrected initial conditions corresponding to the last iteration.
- Maximum error between the initial and final states of the system, i.e. the decision parameter to check convergence.
- *Floquet multipliers* of the periodic solution corresponding to the last iteration.
- A flag that is triggered when the maximum number of iterations have been reached.

Figure 3.1 below includes the flowchart of the algorithm, where:

- $\xi_{\mathbf{i}}$ corresponds to the set of initial conditions at the $i-th$ iteration.
- $\bar{\bar{M}}$ is the *Monodromy* matrix of the system around the trajectory given by $\xi_{\mathbf{i}}$.
- $\mathbf{x_s}(T_0)$ is the final state of the system after a period (T_0).

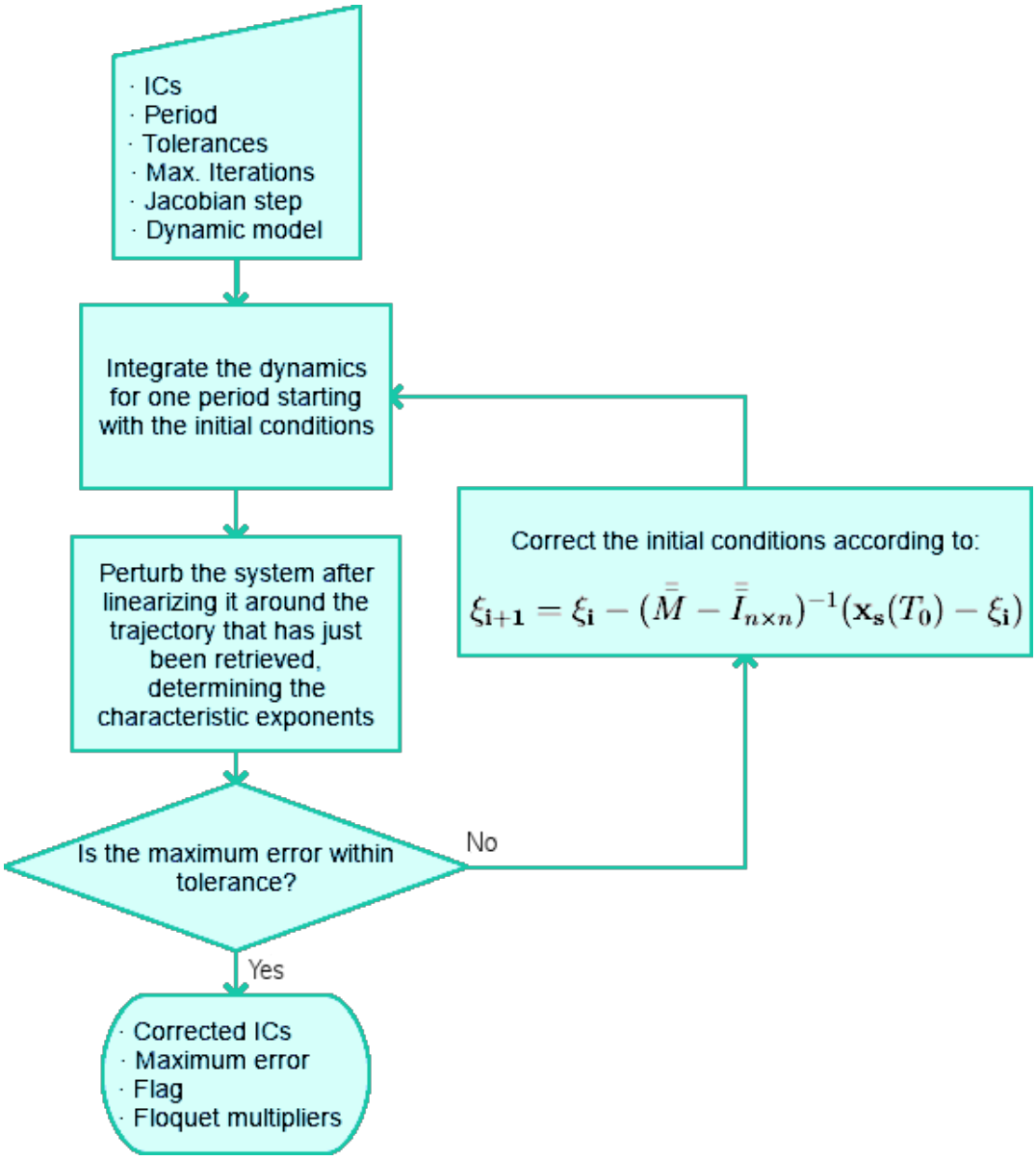

Figure 3.1: Periodic Orbit solver Flowchart.

3.3 Periodic Orbit Example

The current section will cover the first goal of the project, namely, obtaining a valid FOE. For this purpose, the control scheme depicted in figure 2.4 will be used. As it was previously inferred, the very first task consists in retrieving a proper set of initial conditions. Initially via a trial and error procedure until an apparently adequate enough set of values is found, so that the trajectory resembles a lemniscate at first glance. At some point, the model was implemented in SIMULINK software (see appendix A), which turned out to be a good option for pursuing some useful set of initial conditions since a constant monitoring of the system is possible. The following step is to use the periodic orbit solver introduced in section 3.2, which inherits a set of initial conditions and a period[3], and tries to correct these preliminary values until convergence is found at a specified tolerance.

Table 3.1 includes the control parameters that lead to a corrected orbit given the set of initial conditions aside.

Table 3.1 Sample trajectory parameters

Control Parameters		**Initial Conditions**	
Symbol	**Value**	**Symbol**	**Value [rad]**
δ_{max}	21.5 ^{o}	φ_0	1.646313802682947
τ_1	0.9	γ_0	-0.435667074631795
τ_2	1.2	η_0	0.8316257889566826
		θ_0	-0.20467693306388723
		$\dot{\varphi}_0$	-1.9368748167187628
		$\dot{\gamma}_0$	3.226905973205288
		$\dot{\eta}_0$	0.9017996164434295
		$\dot{\theta}_0$	-0.08933691257628472

The resulting path can be found in the following figures. For the sake of readability, instead of the non-dimensional results of the model, dimensional ones in accordance with table 2.1 will be presented. This feature is already implemented in LAKSA project.

[3] Recall the period of the periodic orbit is given by the control scheme, i.e. $T = 2\tau_1 + 2\tau_2$.

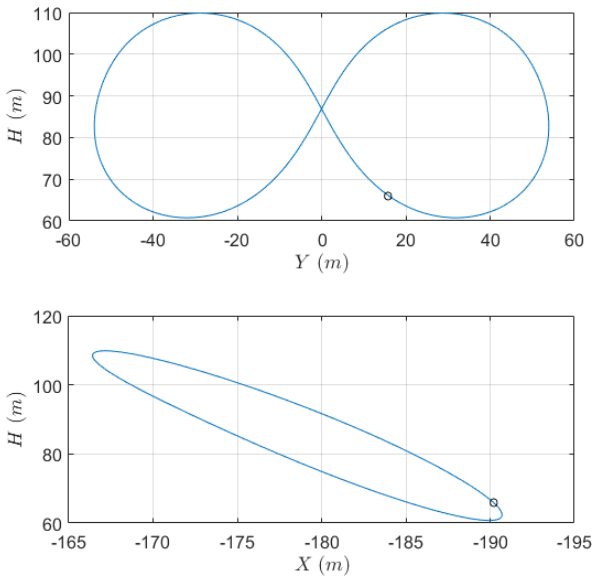

Figure 3.2: Trajectory in the H-Y and H-X planes.

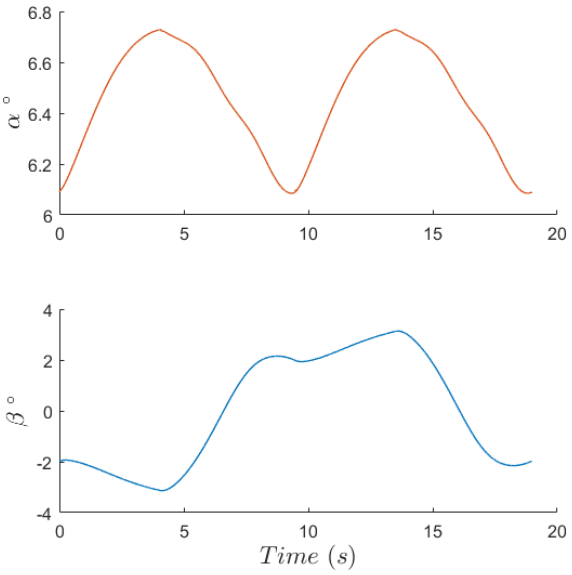

Figure 3.4: Angle of attack and sideslip.

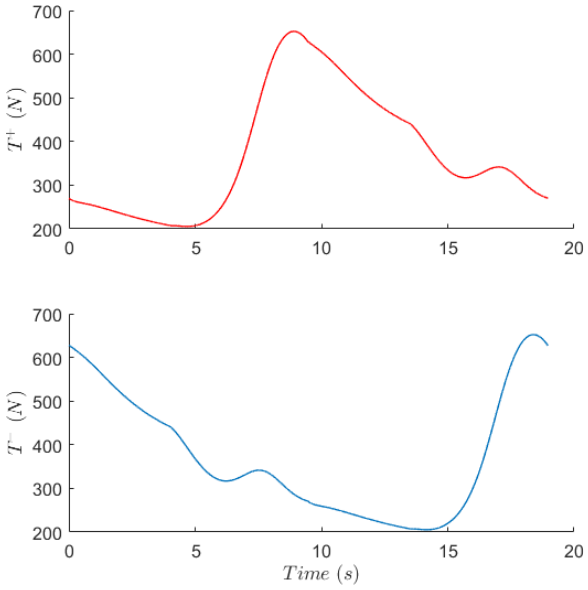

Figure 3.3: Tension produced on each tether.

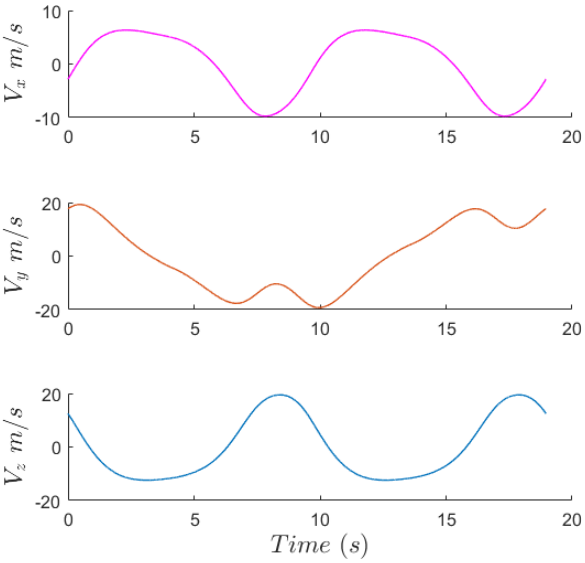

Figure 3.5: Ground velocity components of the center of mass.

Simulation starts from the point highlighted in figure 3.2 towards positive Y values in the upper graph. This figure represents the path followed by the center of mass of the kite, seeming to match a figure-of-eight. The trajectory is symmetric with respect to the wind window, i.e. its center point is located at $y = 0$. Both the outermost turns are notably smooth as reflected by the small variations of the angle of attack in fig. 3.4, of nearly 1 ^{o}. The wind velocity selected for this simulation was 7 m/s, and the maximum speed reached by the kite, 24 m/s, is more than thrice this value. This factor is clearly

below the seven times suggested in section 2.1.2 but by taking a look at the range of the sideslip angle, one may argue that the trajectory can be significantly widened (at least until β reaches $8-11\ ^o$). Maximum ground speed indicated before, resulting from the values included in figure 3.5, is coincident with the maximum tension at one of the tethers: see fig. 3.3. At this point, the tension in one tether is more than two times that on the other due to this instant corresponding to an almost maximum control deflection at maximum airspeed. As $|\delta|$ increases, the kite begins to turn and gain altitude so airspeed and therefore tension are reduced.

Figure 3.6 shows the *Floquet multipliers* of the periodic orbit, which shall be strictly less than one if any damping of the perturbation occurs, i.e. the orbit is stable. This is indeed the case, so that it is a sufficiently valid orbit at first glance. Note that analytical trajectories defined around this orbit may be well followed attending to the relatively good convergence indicated by its eigenvalues.

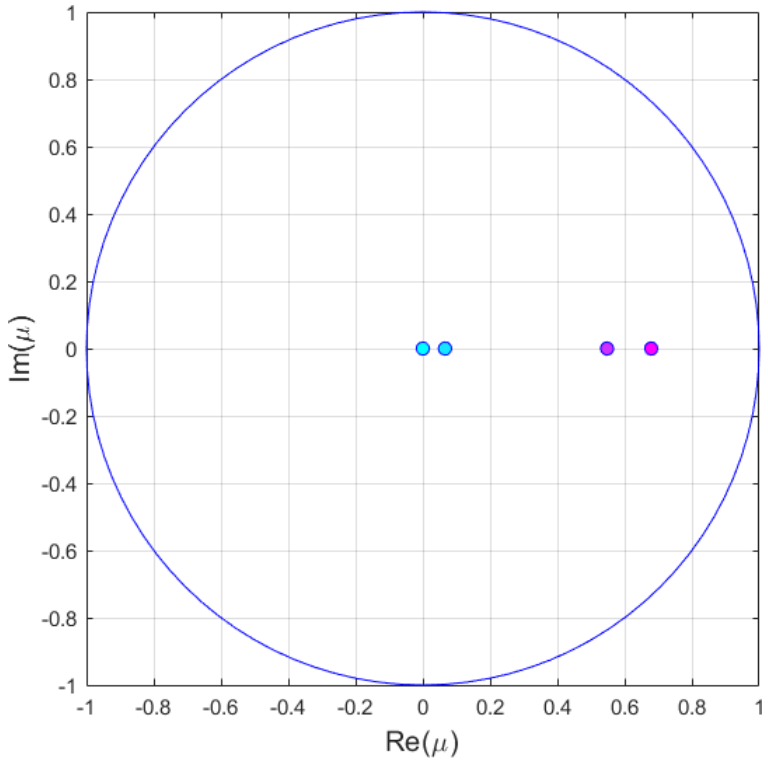

Figure 3.6: *Floquet multipliers* (μ) in the imaginary plane.

3.4 Parametric Analysis

The family of periodic orbits that stem from the variation of the control parameters stated in 3.1 will be thoroughly discussed in the present section. It will serve as an initial approach to estimate up to which point the defined control schedule is capable of adapting to any possible layout provided by use of 2.7 and 2.8. Moreover, the *Floquet multipliers* evolution with the control parameters will be assessed, yielding the stability characteristics of the periodic orbit family.

Recalling that the current model is based on controlling two-line kite solutions aimed at wind energy harvest, it is of paramount importance to inspect how the mean tether tension[4] is affected by the previously mentioned changes in δ_{max}, τ_1 and τ_2. Angle of attack and sideslip will still be supervised even though it has been observed that in the basic trajectory (shown in Fig. 3.4) they lie well below the aerodynamic model limits of validity. The MATLAB routine defined for such analysis inherits the initial conditions corresponding to the periodic orbit that has been previously found and varies some control parameter. Then, it invokes the same predictor-corrector algorithm introduced in section 4.2 in order to retrieve the corrected initial conditions, which will then be introduced as a "guess" for the following step variation in that parameter. It would have been interesting to reach a complete study in terms of stability for each parameters, i.e. the value at which the modulus of some *Floquet multiplier* reaches unity - if any. However, the high computational cost of this task limited the study to the vicinity of the former FOE. Table 3.2 below summarizes the parametric study.

Table 3.2 Control Parameters relevant figures

	δ_{max} ^{o}	τ_1	τ_2
Reference	21.5	0.9	1.2
Range	20.6-22.8	0.68-1.12	0.98-1.42

It may well be noted that the range of variation of δ_{max} ($\approx 10\%$) is considerably narrower than that of τ_1 ($\approx 49\%$) or τ_2 ($\approx 37\%$). The underlying reason of this fact stems from its high impact in the periodic orbit characteristics. This was anticipated by the significant initial error indicated by the periodic-orbit solver for small δ variations, $\Delta\delta_{max} = 0.2$ ^{o} lead to approximately the same error in the first iteration than $\Delta\tau_{1,2} = 0.02$, caused by a remarkable deviation of the trajectory from the reference one. The following set of figures show an evolution over Fig. 3.2 as a result of the parametric study.

[4] The mean tether tension is defined as: $\overline{T} = \frac{1}{\tau_0}\int_0^{\tau_0} T(\tau)d\tau$, where τ is the non-dimensional time and τ_0 is the orbit period.
N.B.: the mean tension in both tethers must coincide because all the trajectories are recurrent and symmetric and the wing is assumed to be flying symmetrically with respect to the wind window.

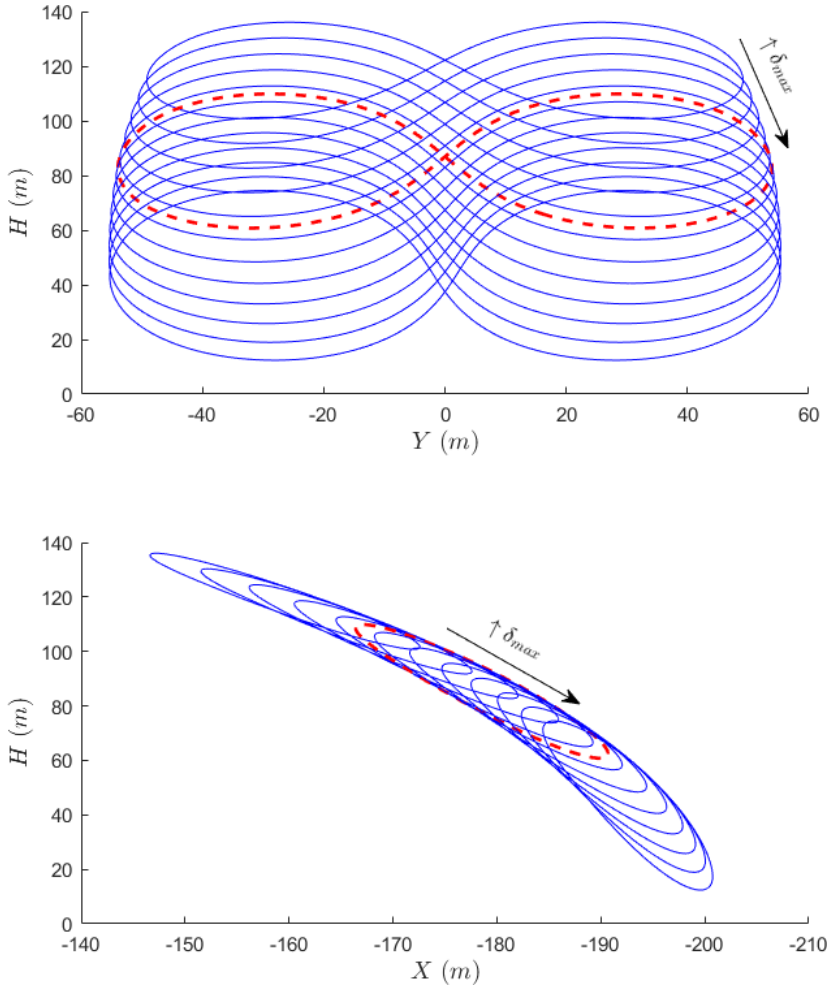

Figure 3.7: Family of orbits for $\delta_{max} \in [20.6, 22.8]$.

Figure 3.7 may indicate that the maximum control deflection is related with the "aspect ratio" (width to height) of the FOE and its elevation. The higher the δ_{max}, the lower the elevation and the "aspect ratio". This is due to a greater difference in tether lengths (with constant ℓ) yielding a faster turn rate and, in principle, the lower the altitude of the kite, the higher the control actuation to perform the same kind of maneuver. This last fact is thought to be related with the higher (kinetic) energy of the system, note that a lower elevation implies a closer scenario to pure crosswind conditions, i.e. wind velocity only providing induced angle of attack.

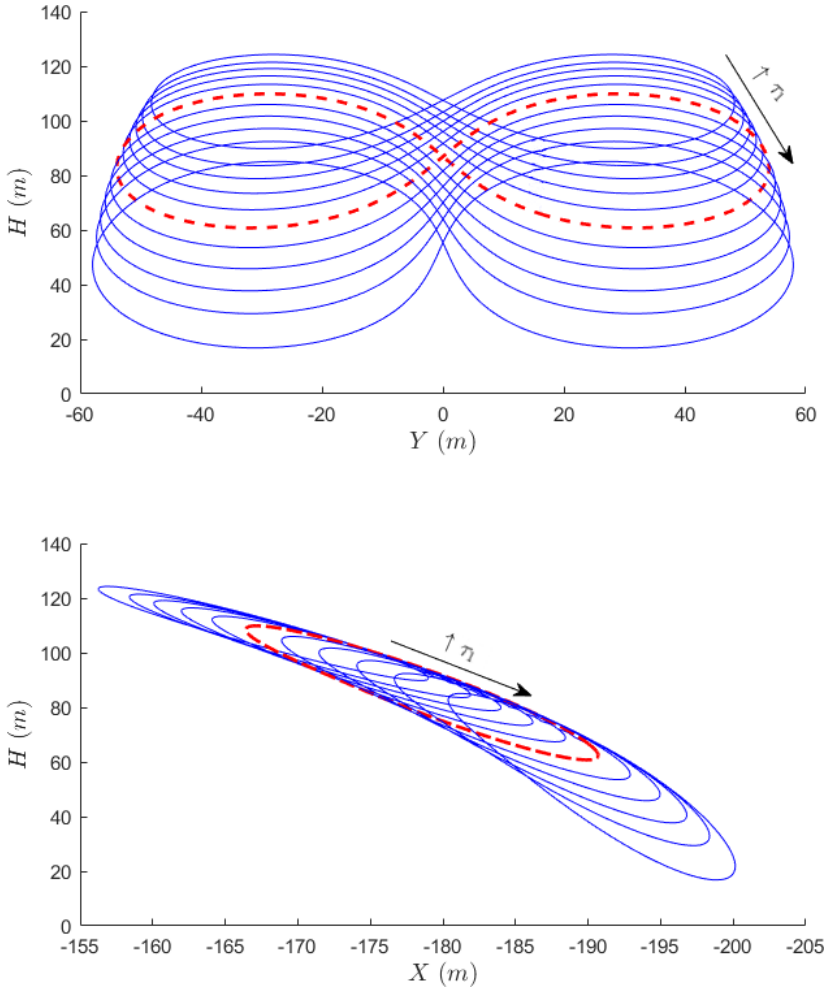

Figure 3.8: Family of orbits for $\tau_1 \in [0.68, 1.12]$.

τ_1 on the other hand, has been found to hold further implications in the overall orbit geometry. Since it is the duration of the maximum control actuation, its effectiveness in controlling the aforementioned "aspect ratio" of the trajectory is greater than that of δ_{max}. Note that in doing so, the altitude of the trajectory is less affected by this change, supporting the previous discussion about a greater actuation requiring a higher amount of kinetic energy available to the system (in exchange for potential one) in order to reach a convergence for the periodic orbit.

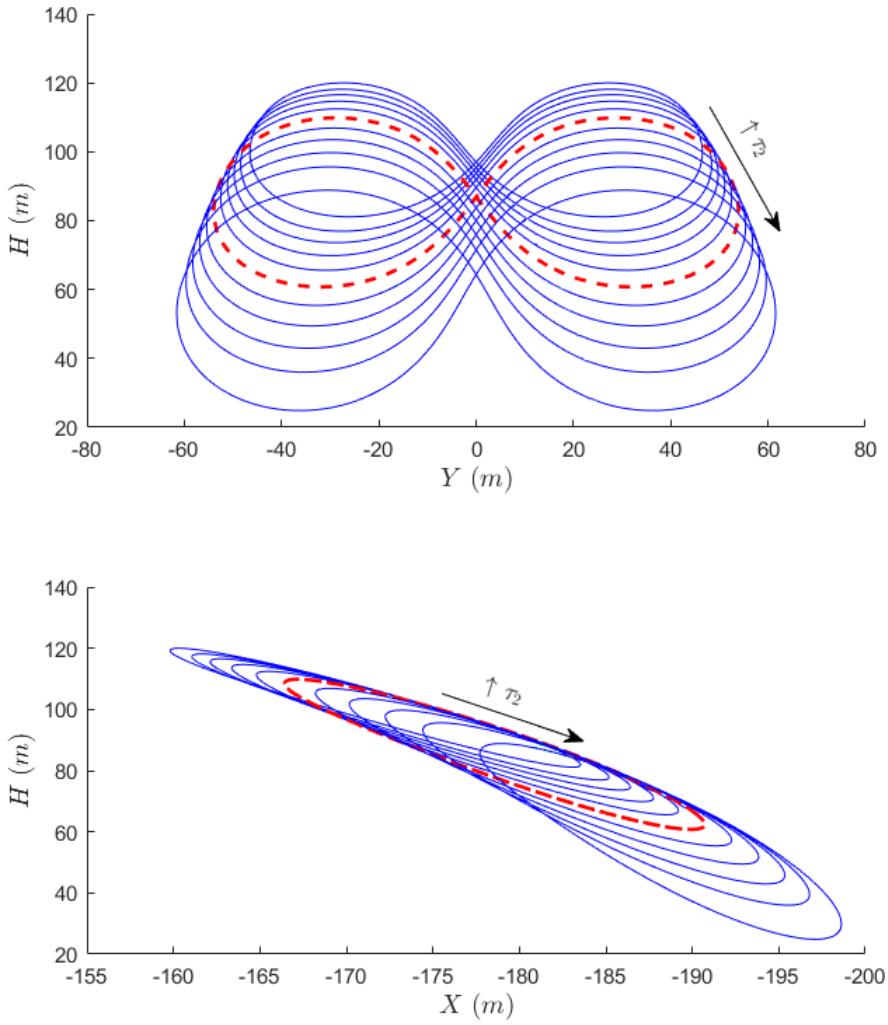

Figure 3.9: Family of orbits for $\tau_2 \in [0.98, 1.42]$

Figure 3.9 shows quite an interesting behavior that highlights the importance of τ_2. Recalling that the latter is simply the transition time between maximum positive and negative control actuations, the dependency of the orbit on this parameter almost entirely lies in its size. A longer transition time implies an enlarged orbit, whereas the "aspect ratio" roughly remains unchanged. It is true that the elevation of the FOE is decreased but this might again be caused by the necessity of slowing the turn rate to accommodate the orbit for this slower transition. Therefore, while δ_{max} and τ_1 feature similar impacts on the periodic orbit, τ_2 is a great candidate to allow for the adjustment of the control scheme that may require a predefined trajectory.

This is to say that τ_1 can be tuned to yield a given height to width ratio, while τ_2 can be used to size the figure-of-eight. Thus, the only parameter that is left to play with, δ_{max}, shall be calibrated so as to reach the required mean altitude and assure the orbit is in fact periodic.

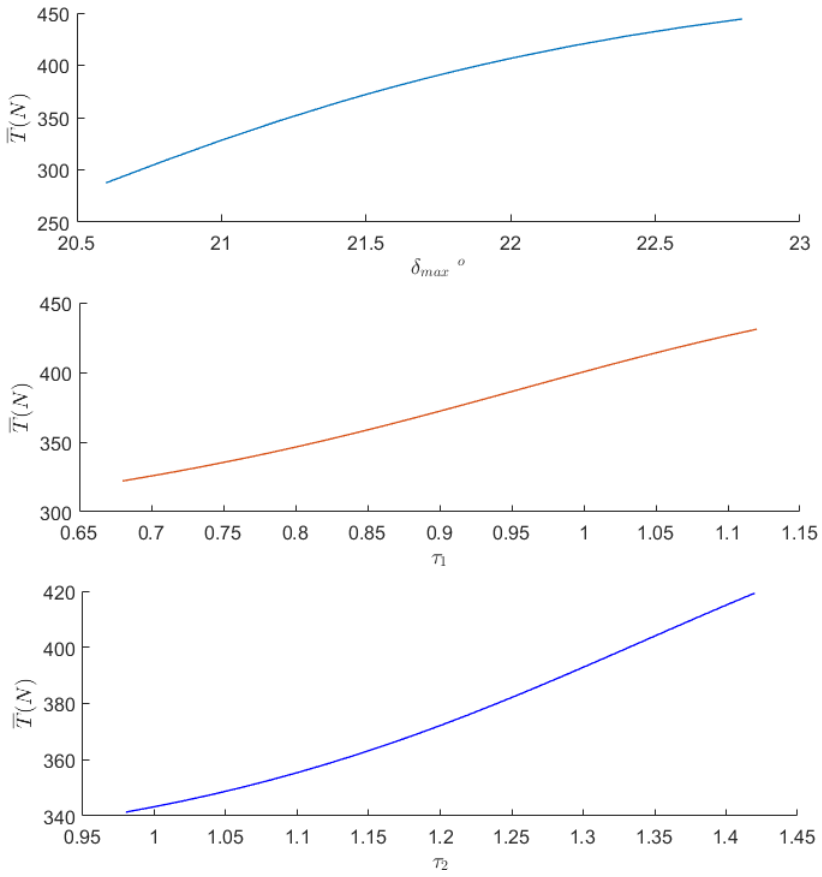

Figure 3.10: Mean orbit tension $\overline{T}$ sensitivity to control parameters.

In the current section introduction it has been stated that the mean tension throughout the periodic trajectory is a main concern due to the intended applications of the system. In this regard, fig. 3.10 is included above in order to derive some preliminary conclusions about the evolution of $\overline{T}$ with the parameters of the presented control schedule. It must be recalled that the non-linearities of the model require simulations in order to identify some trends that might be helpful even in the design of the lifting devices. These trends can not be fully verified neither validated without results and conclusions of parallel studies in these matters.

Two phenomena have been found to imply an increase in the mean tension:

- An extended orbit period in general, either by increasing τ_1 or τ_2, means flying in crosswind conditions for longer. This is in accordance with the ideal scenario introduced in section 2.1.2, where pure crosswind steady state was considered to estimate the maximum power output.
- Flying at lower altitudes essentially implies an injection of kinetic energy in the system. In addition, since wind is supposed to be blowing parallel to the horizon, the angle of attack felt by the kite raises.

The final study prior to the implementation of a path controller consists in assessing the evolution of the stability parameters (i.e. *Floquet multipliers*). The main goal is to find stabilizing and destabilizing regions and whether there exist bifurcations.

The characteristic multipliers shown in figure 3.6 of section 4 turned out to be all real and positive, and this is still the case. Fig. 3.11 below shows their development in the complex plane only for δ_{max} variations. Despite the fact that the actual numerical values do consider complex values, they belong to such a small scale $\sim O(10^{-15})$ that they can be considered numerical errors[5].

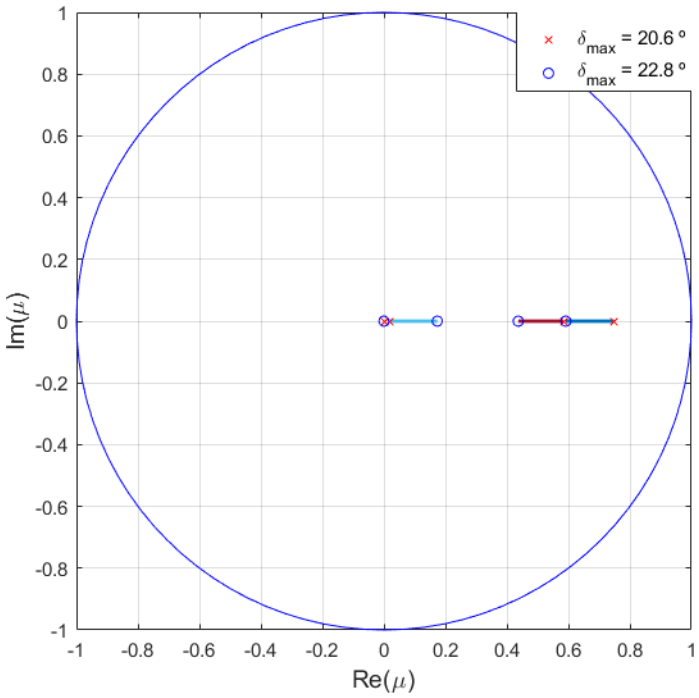

Figure 3.11: *Floquet multipliers* sensitivity to variations of δ_{max}.

[5] The overall tolerance of the study is $\sim O(10^{-6})$ so figures below this order of magnitude are assumed to be numerical zero values.

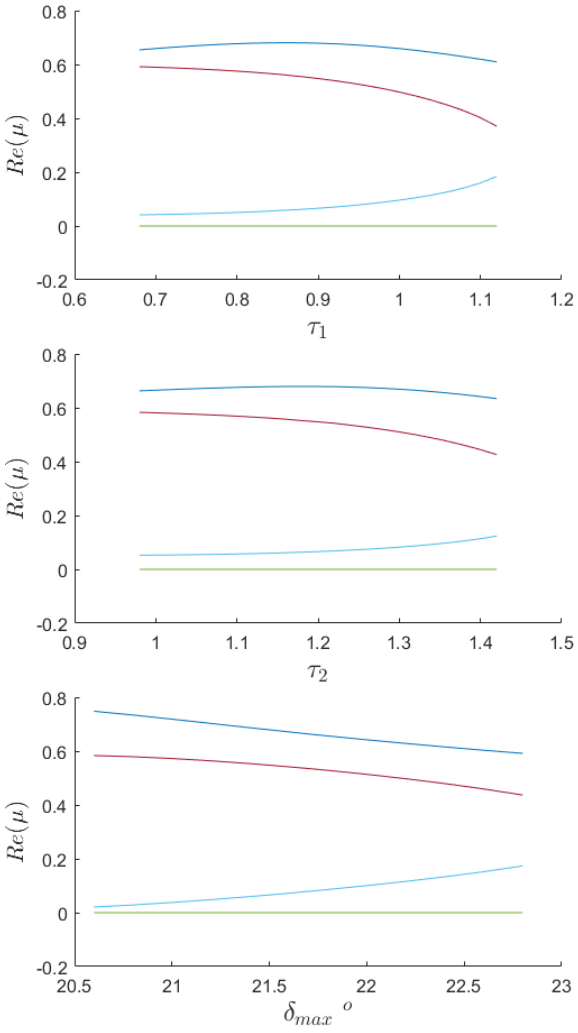

Figure 3.12: *Floquet multipliers* sensitivity to control parameters.

Figure 3.12 aside essentially depicts the variation of the main three *Monodromy* matrix eigenvalues ($\mu_{1,2,3}$) with τ_1, τ_2 and δ_{max}. The largest multiplier μ_1 seems to reach a maximum at the former values of both time steps, i.e. those of the example given in section 4.2, whilst δ_{max} seems to have a linear influence over it. Both μ_1 and μ_2 are found to decrease with altitude for the studied region, and their decrease appears to be absorbed by an increasing μ_3.

Nevertheless, this study might not be applicable to every figure-of-eight definition since the ranges of variation of the control parameters are not large and the resulting periodic orbits are very close to one another. A deeper understanding on these matters might be retrieved after a fully functional controller is achieved.

The only remarkable result of this stability analysis is its relatively smooth behavior of the characteristic multipliers on the whole periodic orbit family. This suggests that a wide variety of lemniscates can be safely flown in this region.

4 | Path Controller

4.1 Initial Objective

The final aim of this project is to implement a controller capable of following a predefined target. Now that a validated FOE has already been obtained, the first step is to tune the parameters of the analytical trajectory defined in section 2.3 to resemble the periodic orbit example presented in section 3.3. Such values are summarized in table 4.1 below.

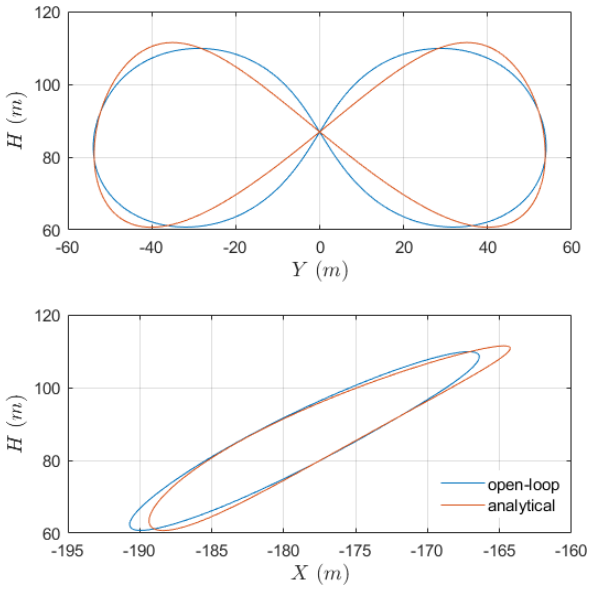

Figure 4.1: Target vs open-loop FOE

Table 4.1 Analytical trajectory parameters

Symbol	Value
λ_1	$25\ ^o$
λ_0	$8\ ^o$
χ_0	$17.5\ ^o$

Figure 4.1 aside includes the z-y and z-x projections of both trajectories. Even though there are clear similarities between them, some crucial differences can be observed. The sharper outer turns may require more aggressive control actuations. The linearity of the inner cross might as well trigger difficulties in terms of controllability, possibly resulting in a remarkable increase over the maximum accelerations of the former open-loop scheme.

4.2 CasADi [3]

During a visit to *Albert-Ludwigs-Universität Freiburg*, the supervisor of the present work was able to adapt the matlab model to **CasADi** in the form of an optimal control problem. This open-source software is mainly focused on numerical optimization and optimal control. It is based on a symbolic framework that makes it an efficient *Algorithmic differentiation* (AD) tool. The main difference between **CasADi** and former AD tools is that codes already implemented in MATLAB or Python need moderate to vast modifications to adapt them to **CasADi** syntax. One can find a complete user guide contains an in-depth explanation on how to adapt a given user code written in C++, Python or MATLAB to this tool's syntax[1]. Moreover, it includes a list of the diverse problems that can be addressed and the different approaches or building blocks implemented in **CasADi** software.

4.2.1 Optimal Control Method

Some modifications of the model are required for the optimal control problem to be properly posed. It has been stated that the system is an implicit function of the second derivative of the control vector. Accordingly, one may define an extended state vector $\mathbf{x_{s,amp}}$ and a new control vector u_c as follows:

$$\mathbf{x_{s,amp}} = \begin{pmatrix} \varphi & \gamma & \eta & \theta & \dot{\varphi} & \dot{\gamma} & \dot{\eta} & \dot{\theta} & \ell & \delta & \dot{\ell} & \dot{\delta} \end{pmatrix} \tag{4.1}$$

$$\mathbf{u_c} = \begin{pmatrix} \ddot{\ell} & \ddot{\delta} \end{pmatrix} \tag{4.2}$$

This formulation prevents inconsistencies that may arise in the former system between the control vector and its derivatives. Due to the complexity of the model, conversion from its initial continuous time to discrete time dynamics was avoided. Instead, a **Direct Collocation Method** was used to obtain the control law that allows the state variables to follow a predefined target trajectory, using the primal-dual interior point algorithm (**ipopt**) developed by Andreas Wätcher et al. in [27]. For this purpose, it is necessary to discretize a path similar to the target one, upon which modifications will be performed so to minimize the differences between them. Therefore it is necessary to convert the model from time-based (τ) to arclength-based[2] (s) integration:

$$\frac{d\mathbf{x_{s,amp}}}{ds} = \frac{1}{||\dot{\mathbf{x}}_{\mathbf{cg}}||}\mathbf{f}(\mathbf{x_{s,amp}}, \mathbf{u_c}) \tag{4.3}$$

The latter procedure is straightforward since the only dependency of the model in time was through the controls, which are now considered unknowns and must be compliant with the target state of the system.

[1] https://web.casadi.org/docs/#document-ocp

[2] The arclength parameter s is defined as $s = \int ||\dot{\mathbf{x}}_{\mathbf{cg}}|| d\tau$, where $||\dot{\mathbf{x}}_{\mathbf{cg}}||$ is the velocity of the center of mass of the kite with respect to the earth fixed reference frame S_E.

Discretization of the base trajectory is performed at two different levels:

- **Control or Main Mesh:** a coarse mesh at the control level. Control values are assessed at each point.
- **Sub-Mesh:** finer mesh that propagates the dynamics for the fixed control values given by the *Main Mesh* between two consecutive points of the latter. It is basically used to allow a fast and efficient integration method, in the current case through 3^{rd} order *Legendre* polynomials[3].

Please note that each collocation point completely defines the state of the system in terms of state and control variables as well as covered arc-length.

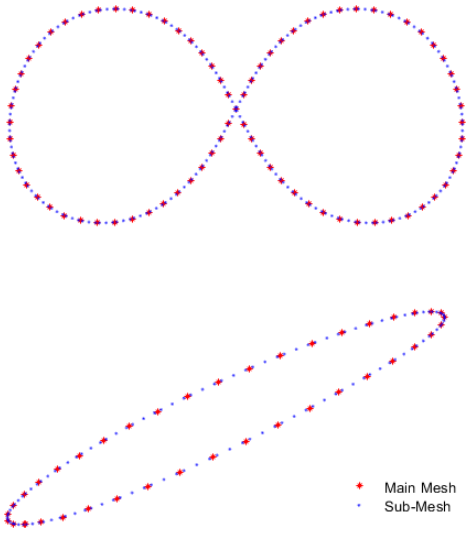

Figure 4.2: Base trajectory discretization

Figure 4.2 depicts the discretization of the base trajectory (fig. 3.2) for 81 collocation points in the *Control Mesh*. For simplicity, all the points in either the main or the sub mesh shown are equispaced. A more efficient layout may be based on the output of the ODE solver used, properly tuning the absolute and relative errors to limit its fineness. In practice, the grid spacing selected was uniform since a layout given by the ODE solver may imply a high computational cost. Considering the current project as the implementation but not thorough discussion of a path controller, the selection of equal spacing is sufficiently accurate.

4.2.2 Cost Functional

Optimal Control is based on minimizing a cost functional. This functional must include all the relevant target parameters and adequate relations between them and the state of the system. A tracking example may be given by:

$$F = \int k_r ||\mathbf{x_{cg}}^* - \mathbf{x_{cg}}|| + k_\zeta ||\boldsymbol{\zeta}^* - \boldsymbol{\zeta}|| + k_0 ||\mathbf{x_{cg,mid}}^* - \mathbf{x_{cg,mid}}|| + k_{reg}(\boldsymbol{\omega} \cdot \boldsymbol{\omega}^T) \quad (4.4)$$

Where:

- The superscript * refers to the target trajectory
- $\boldsymbol{\zeta}$ is the direction of the velocity vector, i.e. $\boldsymbol{\zeta} = \frac{\dot{\mathbf{x}}_{\mathbf{cg}}}{||\dot{\mathbf{x}}_{\mathbf{cg}}||}$

[3] *Legendre* polynomials are the solution to *Legendre*'s differential equation and are often applied to non-linear differential equations solvers [12]. They are given by $P_n(x) = \frac{1}{2^n n!}\frac{d^n}{dx^n}(x^2-1)^n$.

- $\boldsymbol{\omega}$ is the so-called decision vector, used to improve the convexity of the problem. It is composed by the state and control vectors, i.e. the decision variables of the system.
- The mid point of the trajectory is emphasized at both crossings with a separate weight constant k_0.
- *Delta*, whereas not included in equation 4.4, is a **CasADi** parameter used to ensure periodicity of the solution, also having an associated constant k_Δ.

One has to play with the five different weights to emphasize on the importance of their corresponding parameters, bearing in mind that a high k_{reg} may eventually imply a deviation from the target trajectory.

4.2.3 Constraints

Direct Collocation Method building block lets the user provide constraints for all variables included in the decision vector. In addition, it is possible to add other type of constraints to functions called within the model or even runtime calculations. The most important constraint is aimed at enhancing the 3^{rd} order interpolation, ultimately leading to as accurate as possible dynamics propagation. It ensures that the predicted values of the state derivatives match those given by the equations of motion in the *Sub-Mesh*.

Some additional constraints are listed below:

- Tension on each tether must always be positive. Indeed some minimum and maximum values are imposed according to the main FOE results and performance of typical tether materials, such as Dyneema® SK99[4].
- Aerodynamic model limits can be added to directly retrieve valid results in this regard.

One can think of these restrictions as guidelines for the optimization, yielding results that are in line with expectations and thus preventing the solver from exploring undesired areas in its search for a global minimum.

4.3 Validation of Results and Convergence Analysis

Depending on the fineness of the mesh and the performance of the *Legendre* interpolating polynomials, the optimized control law may not lead to a periodic orbit. For this purpose, the predictor-corrector algorithm presented in section 3.2 will be provided with the resulting initial conditions and an interpolation routine that outputs

[4] http://www.dsm.com/products/dyneema/en_GB/applications/sports-equipment/paragliding.html

the control value at any given point. An assessment of the characteristic exponents will ultimately yield the degree of applicability of the control law - given that the resulting orbit is in fact periodic. Prior to validation, a convergence analysis shall be conducted, refining the discretization of the base trajectory until no significant variations of the results can be detected via further refinement. This is a reasonable procedure because the finer the *Control Mesh*, the better the optimization. The underlying reason is that the system has more freedom in terms of control scheme.

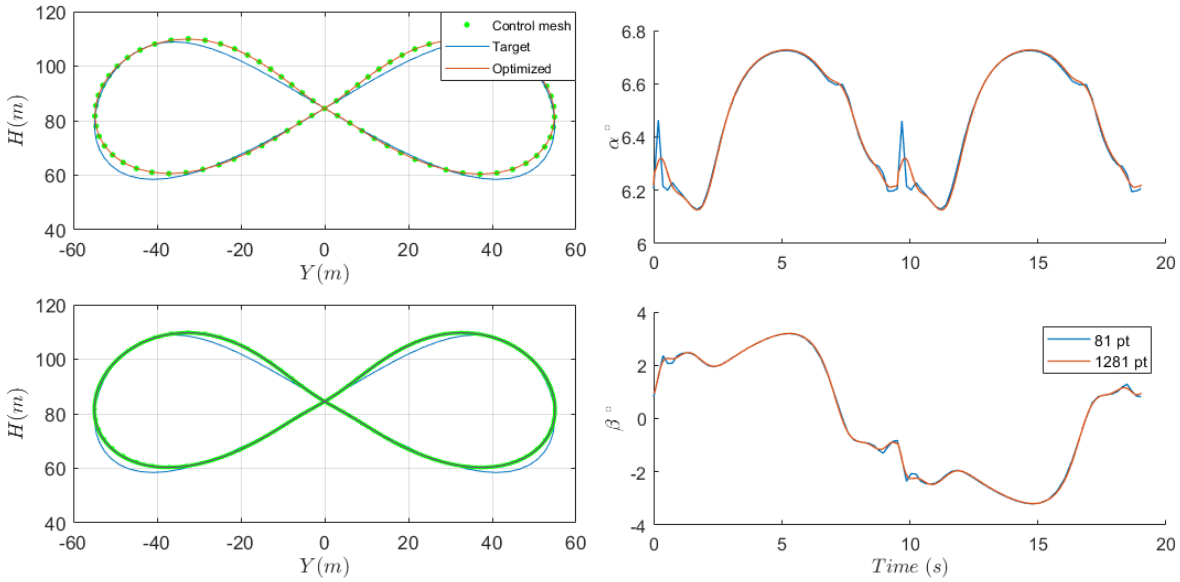

Figure 4.3: Effects of varying the number of collocation points in the *Control Mesh*. 81 points for the upper-left figure and 1281 points for the lower-left one.

This fact can be visualized in figure 4.3, where a significant increase in smoothness in the ressponse of both the angle of attack and sideslip is found when increasing the number of discretization points. Nevertheless, variations are only relevant near the center of the FOE trajectory, suggesting important control actions must be performed to conduct the system through the $Y = 0$ target point. The trajectory in the $Y - H$ plane does not seem to be affected by such variations at least for the two levels of discretization considered. Recalling the cost functional is focused on minimizing the distance to the target path, the resulting control law may feature important jumps. These jumps have a low impact in the position of the center of mass because the control law determined by the optimization software corresponds to the evolution of $\ddot{\mathbf{x}}_\mathbf{c}$ with time. Therefore, as it can be seen in the evolution of α, an excess positive control actuation is corrected by a strong negative one, rendering a smooth second integral which is the case of $\mathbf{x}_{cg}$.

Figure 4.4 depicts the results of the convergence analysis. The maximum error indicated in the vertical axis corresponds to the maximum difference between the evolution of the state variables as predicted by **CasADi** and those retrieved after propagating the dynamics with a Runge-Kutta 4-5 (ode45) solver[5]. The control law output from

[5] Considering the initial conditions and control scheme determined by the optimization software.

the optimization was interpolated at each integration point by using the option *pchip*[6] in MATLAB 1D interpolation function "interp1". Several approaches were considered besides this one, including truncation of high frequency components by means of Fast Fourier Transforms and the exact stepped control law determined by **CasADi**. However, none of them seemed to perform better than the *pchip* interpolation.

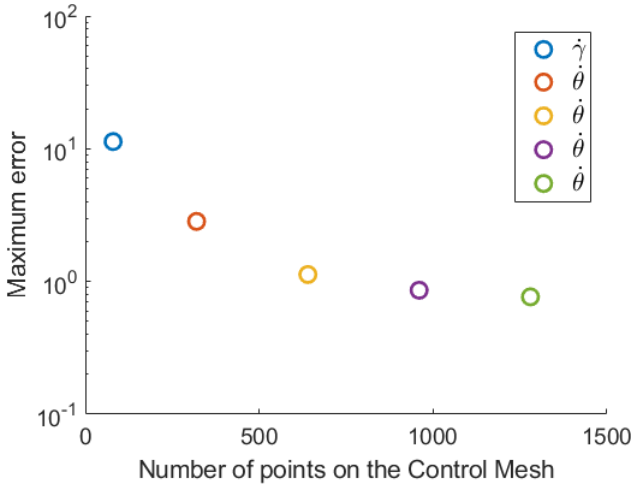

Figure 4.4: Maximum error evolution with grid size[7].

One may argue that although the dependency of the error with respect to the mesh size is barely noticeable between the last two grid sizes (961 and 1281 points respectively), the maximum error is still of order unity. Again considering the 3^{rd} order *Legendre* polynomial approximation used by the solver and the error determination described in the previous paragraph, there are other significant sources of error besides the grid size. Analogously, given a certain level of similarity between the initial guess for the trajectory and the target one, no further optimization can be obtained by selecting a better initial guess. This is to say that if the resulting corrected trajectory is reinserted in the routine, there will be no significant changes in the output since that is the maximum accuracy that can be obtained with such grid size.

4.4 Results and Discussion

The outcome of the path controller implementation will be presented throughout this section. Several figures depicting relevant states of the system are to be discussed, together with the optimized control law. The resulting trajectory in the H-Y plane and aerodynamic angles were already presented in figure 4.3. Please note the first

[6] Piece-wise Cubic Hermite Interpolating Polynomial, refer to MATLAB documentation https://es.mathworks.com/help/Matlab/ref/pchip.html

[7] Legend aside highlights the state variable that exhibited the highest error.

control variable ℓ is kept constant due to the target trajectory lying within a sphere of constant radius.

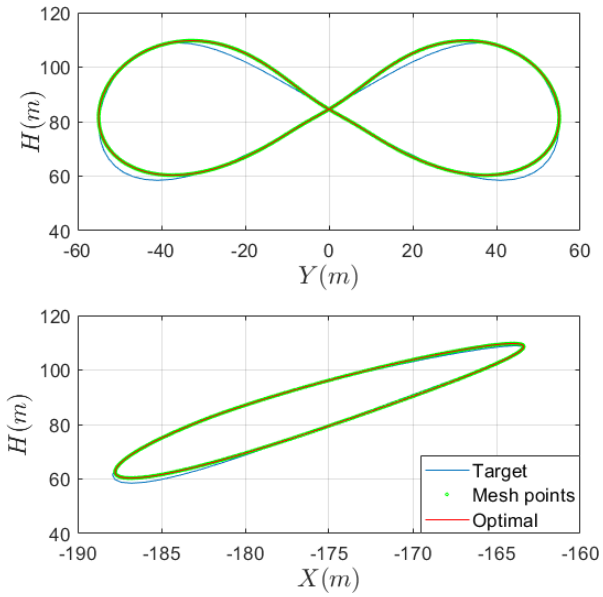

Figure 4.5: Optimal trajectory in the H-Y and H-X planes.

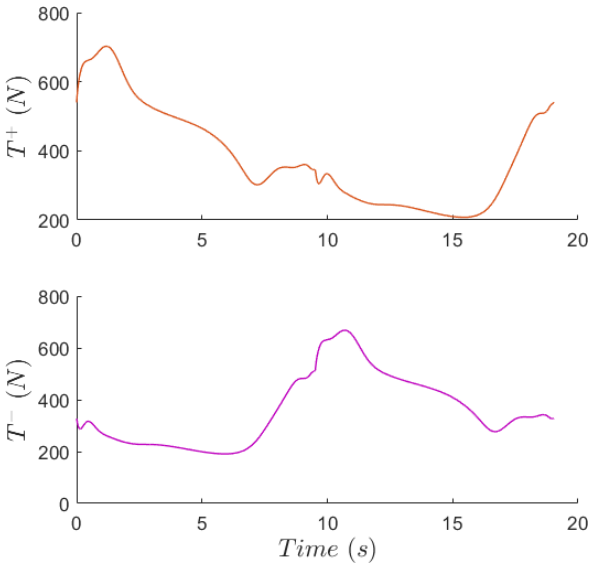

Figure 4.7: Optimal trajectory tensions.

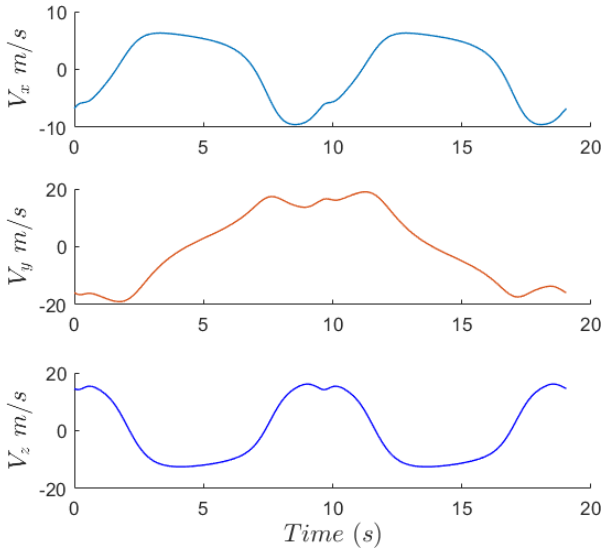

Figure 4.6: Center of mass ground velocities for the optimal trajectory.

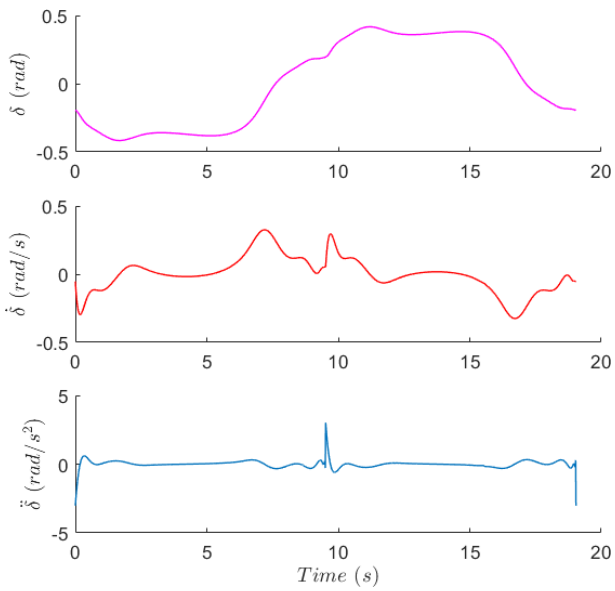

Figure 4.8: Optimal control law.

Figure 4.5 suggests the optimal trajectory is rather close to the target one. Deviations only occur at the initiation of the turns, which is thought to be caused by a weak control influence on the kite attitude. The sharper turns of the target trajectory seem unfeasible for the system, so the lower ones are anticipated and deviations in the upper ones corrected. It is also important to highlight the kite attitude strongly depends on

the absolute wind speed, which has been fixed at a constant 7 m/s for the whole study. Besides the high peak in $\ddot{\delta}$ at the inner crossing of the trajectory, the control law is somewhat smooth. The periodic orbit solver was provided with this control law and initial conditions in order to verify the orbit was periodic, which is in fact not the case. This peak in $\ddot{\delta}$ suggests that an aggressive and sharp control action must be conducted in order to force periodicity. The orbit is then thought to be unstable mainly because it is not periodic. For a real application, an additional controller shall be implemented on-board to mitigate perturbations and also ensure a proper response at the inner crossing of the figure of eight. An assessment of the stability would be more crucial in that case because if the trajectory is highly unstable, the on-board controller might not be able to counteract even small perturbations.

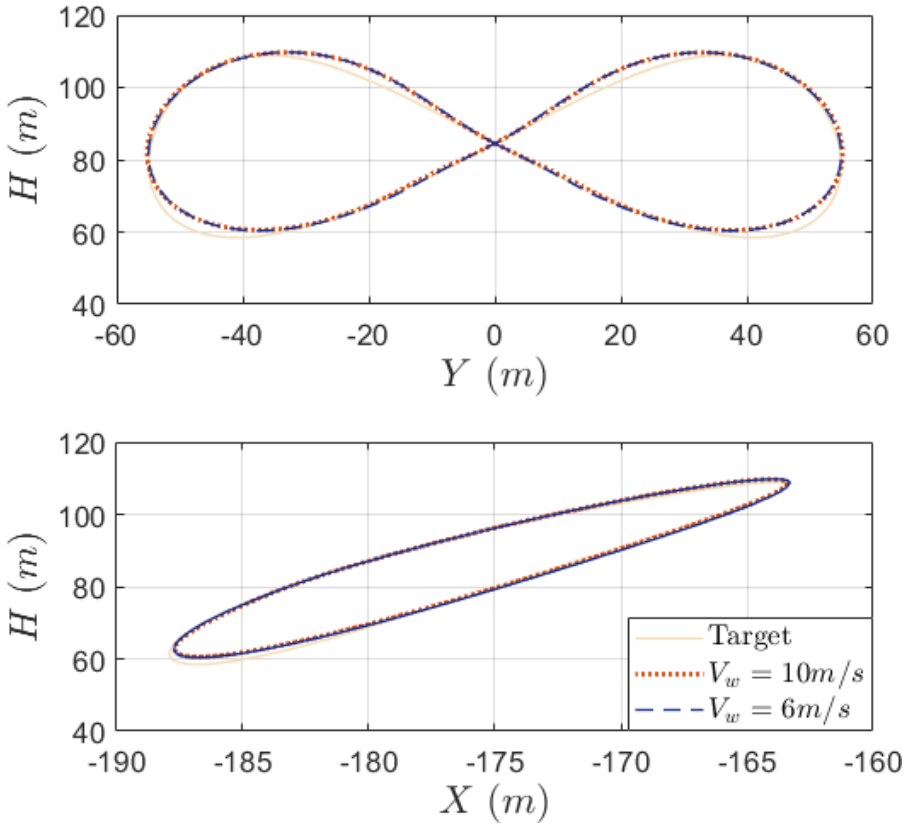

Figure 4.9: Optimal trajectory in the H-Y and H-X planes for the range of feasible wind velocities.

The decision of posing the controller implementation as an optimal control problem turned out to be a rather smart approach. Now it is possible to use the controller as a highly efficient dynamics propagator, which in fact returns the feasibility of following a target trajectory. In this regard, the range of wind speeds for which the controller was able to find an optimal control law, i.e. found a solution, will be discussed. Figure 4.9 illustrates the difference in $\mathbf{x_{cg}}$ path for the two wind speed limits: 6 and 10 m/s.

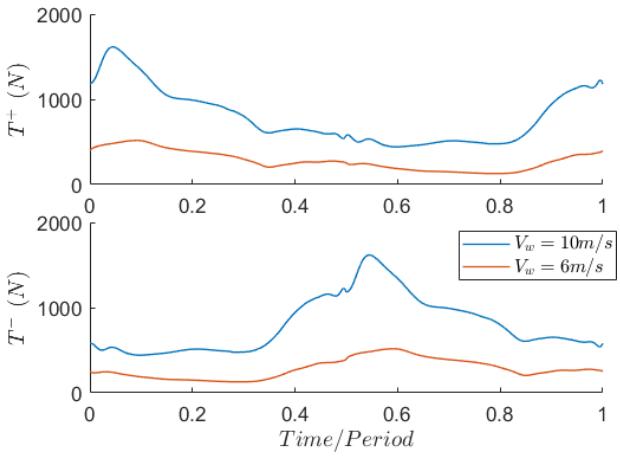

Figure 4.10: Optimal trajectory tensions for the feasible wind speed range.

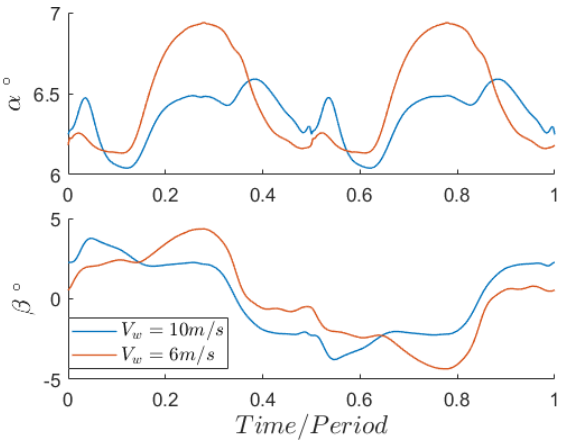

Figure 4.11: Aerodynamic angles for the feasible wind speed range.

Albeit the trajectory for both absolute wind speeds are virtually identical, there are significant differences in the tensions and the aerodynamic angles as it can be inferred from figures 4.10 and 4.11. The increase in tension for higher wind speeds is intuitive and could have been predicted before hand. The change in period due to variations of the wind velocity is dramatic: for $V_w = 6\ m/s$ the period is $T_0 = 22.6\ s$, whilst for $V_w = 10\ m/s$ the period is $T_0 = 13.1\ s$; hence, causing the significant difference in maximum tension. The sideslip angle β does not seem to behave differently in both cases, so the relative lateral wind speed felt by the kite is similar. The latter fact can be understood as the kite behaving similarly at the turn maneuvers regardless of the wind velocity for a given target trajectory. Conversely, it can be inferred from the evolution of α that the increase in absolute airspeed is steeper than the increase in the wind reference velocity. This is to say that an increase in the wind reference speed triggers a higher increase in the wind velocity felt by the kite, which can also be derived from the significant decrease in the period.

Another interesting branch of solutions is achieved by varying the mean altitude of the trajectory. Two different cases are presented in figure 4.12, considering mean elevation angles λ_1 of 40 ^{o} and 15 ^{o}. Indeed, conclusions reached after the wind reference velocity were applied. At first, a control law compliant with a target trajectory featuring $\lambda_1 =$ 40 ^{o} could not be found, ergo the reference wind speed was increased from 7 to 10 m/s. This suggests that the kite maneuverability increases with the reference wind speed and the range of feasible target trajectories is broadened. It was not possible to find control laws that permitted elevation angles beyond this range for the base target trajectory , i.e. $\lambda_0 = 8\ ^o$ and $\chi_0 = 17.5\ ^o$. The applicability of the latter trajectory shape is then limited to the previously mentioned range of wind reference velocities and the current range of mean elevation angles, which starts to depict the solution space in which all the possible trajectories lie.

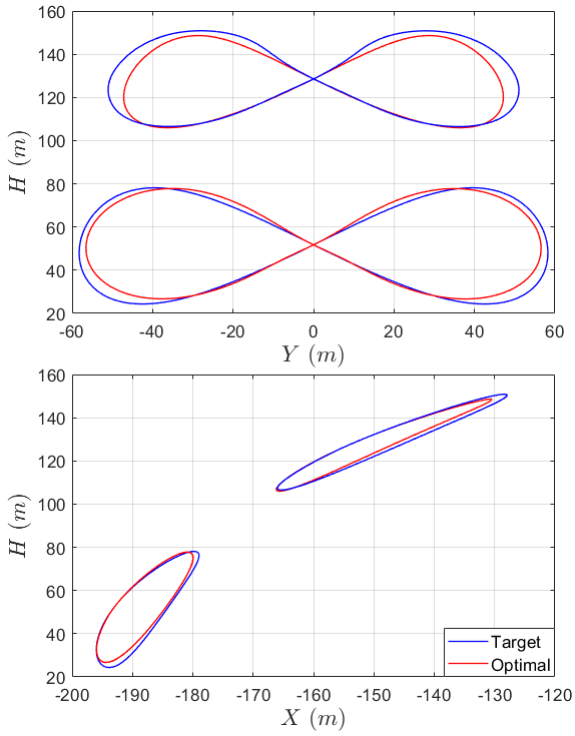

Figure 4.12: Optimal trajectory for $\lambda_1 = \{15, 40\}$ ^{o}.

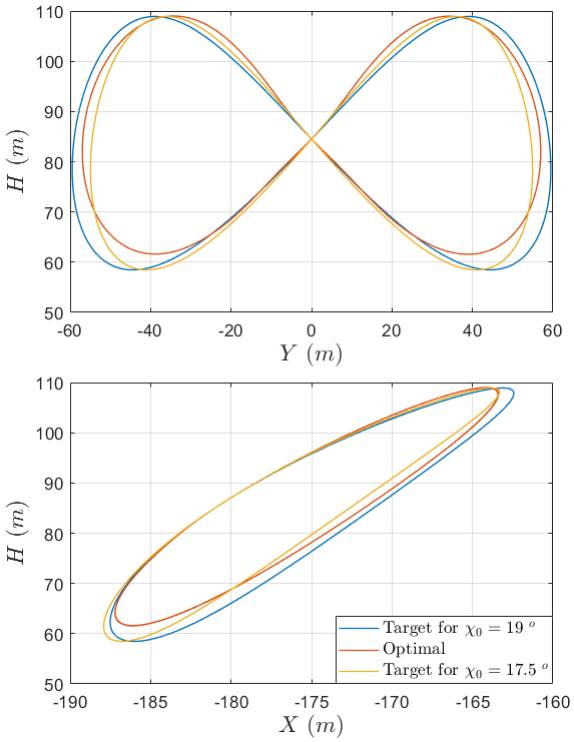

Figure 4.14: Optimal trajectory for $\chi_0 = 19$ ^{o}.

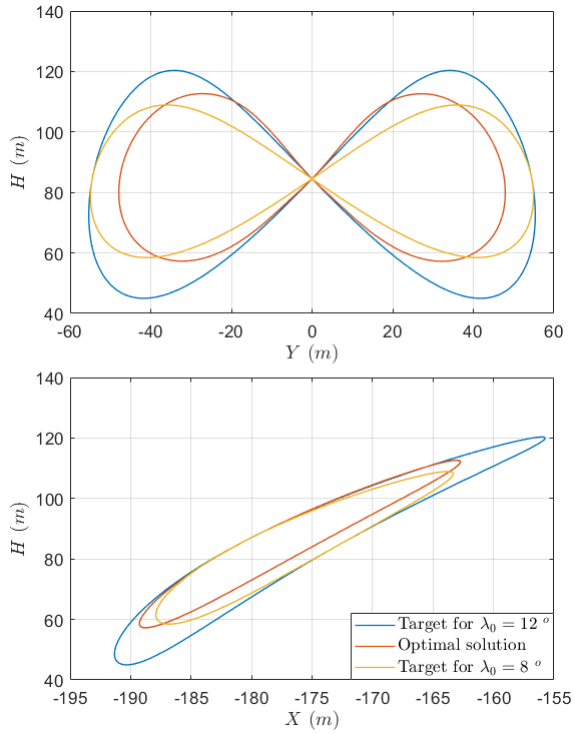

Figure 4.13: Optimal trajectory for $\lambda_0 = 12$ ^{o}.

The solution space will be fully covered by analyzing different layouts for the target FOE, either varying λ_0 or χ_0. Whereas no solution could be found by the optimal control solver for a decrease in λ_0, figure 4.13 shows the optimal trajectory for $\lambda_0 = 12$ ^{o} and $V_w = 7$ m/s. The path tracking for this last orbit is considerably imprecise, and the reason for this was inferred from the first optimized trajectory. These results suggest the system is not able to perform turns sharper than the ones of the former trajectory presented in 4.5. Consequently, no optimal trajectory would be found if χ_0 is decreased, rendering the controller unable to find trajectories with lower arc-length. There are still no strong arguments besides this limit for the turning radius. For the sake of completeness, figure 4.14 depicting a trajectory with $\chi_0 = 19$ ^{o} is included above.

4.5 Concluding Remarks

Prior to discuss the conclusions extracted from the project, a brief summary of the mi is included in order for provide an overall foundation for such conclusions.

- The very first task of implementing the model into SIMULINK environment is thought to be of aid for later development phases.
- A very important remark regarding kite dynamics is the fact that the real applicable controls of the system are the second derivative of the tether lengths. This is caused by the state vector and thus the attitude of the kite being coupled with the length of each tether and its first derivative.
- Up to this point, a decent knowle on dynamical systems has been developed, understanding control theory from the non-linear approach - opposed to the typical linear problems suggested throughout the *Bachelor*.
- The forthcoming event is the applicability of *Floquet* and autonomous systems theory to the dynamical system of study, with the aim of determining periodic figure of eight trajectories. An open-loop control law consistent with the aforementioned control issue is defined, which rendered a periodic orbit with the aid of a predictor-corrector algorithm.
- Such algorithm, apart from adapting the set of initial conditions to yield a periodic orbit, also determines its *Monodromy* matrix and *Floquet multipliers*. The latter fact directly allows a linear stability analysis.
- Next step is to perform a parametric analysis on the control law that allowed a periodic figure of eight. Such analysis revealed that there is a wide variety of stable periodic orbits, hence suggesting the controller could be capable of tracking target trajectories of different shapes.
- A proportional derivative velocity direction based controller is implemented in the SIMULINK model without sucecss. Non-linear Dynamic Inversion is developed for this control scheme to account for the non-linear response of the system to controls, not leading to meaningful results neither. Nevertheless, during this implementation some intuition on the dynamical system is developed, together with a useful non-linear control scheme: proportional integral derivative control corrected by non-linear dynamic inversion.
- Controller was thereafter converted into an optimal control problem by using a **Direct Collocation Method** in the **CasADi** software environment. By means of this tool it is posible to track different analytical target trajectories.
- A preliminary study on the capabilities of the optimal control solver was conducted, starting to depict a solution space of feasible target figure of eight trajectories. Effects of wind reference velocity are also analyzed up to some extent, and higher wind speeds seem to allow for a better controllability of the system.

Albeit a run time path controller could not be implemented, the choice of a controller in the form of an optimal control problem has possibly shed more light in understanding the two-line kite model dynamics and response to controls. Merging the model in SIMULINK is thought to aid the parallel work of hardware-focused projects. Despite the proposed velocity direction based controller (see appendix A) not being able to properly track the desired path, it may be recalled once on-board perturbations are to be mitigated. With regard to power generation, the current kite configuration seems to be barely applicable since initial conditions are, up to this point, key in order to follow a target path. Recalling the dynamic system of interest does not feature depowering capabilities, performing the reel-in phase in a flaggered state would introduce an unfeasible level of uncertainty, resulting in a rather unefficient reel-in reel-out duty cycle. Traction applications seem to be the target niche for two-line kite systems. Notwithstanding, a carousel-layout system that does not require a reel cycle and only relies on traction to generate power is still a valid yet complex application.

A solution space for the optimal control problem has been sketched. In fact, the cases for which optimal trajectories were not found may not necessarily lie outside the range of physical solutions inherent to the model. The initial guess for the all the scenarios presented in section 4.4 was the example trajectory introduced in section 3.3, and the dependency of the optimal control problem solution space on the initial guess has yet to be analyzed. This last point could broaden the range of applicability of the optimal control problem, and is expected to happen based on the outcomes of the parametric analysis (section 3.4). Such analysis revealed there is a significant diversity of stable periodic orbits accessible to the system.

4.6 Future Work and Recommendations

Continuing with the discussion of the solution space for the optimal control problem, there is yet a lot of research pending before considering to design an on-board controller for perturbance mitigation - which shall indeed account for stochasticity issues. The possible branches of study that stem from the current project may thus read:

- Analyze the impact of varying the initial guess on the optimal trajectory found using the current **Direct Collocation Method**.
- Given the solver solution space is affected by such variations, continue searching for feasible solutions with the aim of assessing the capabilities of two-line kite configurations.
- Since reel-in reel-out applications have been found impractical, modify the cost functional to maximize the mean tension.
- Related to maximizing tension for traction applications, explore the possibility of defining trajectories with some shift in the y-axis, which essentially implies adding some $\chi_1 \neq 0$ (analogous to λ_1) in the target trajectory definition.

- Try to find optimal trajectories that whilst starting at some arbitrary initial condition or even the equilibrium point, end at a desired state. If such possibility exists, the system could be easily initialized in order to follow a figure of eight. Recall the simulink model provides an adequate environment in this regard.
- Another interesting area of study is the wind velocity field. Some wind gradient included in LAKSA project was considered, unfortunately the solver was not able to provide a feasible control law for such environment.

Related to these items, some recommendations and caveats arose throughout the development of the current project, which are throught to be of aid to future researchers. The author does not consider them dogmas, but such suggestions are based on the expertise acquired during this preliminary research on the optimal control problem capabilities.

- With regard to maximizing the tension, some additional constraints should be considered. It has been observed that leaving $d\ddot{e}lta$ unconstrained, the optimal control solver tends to include sharp variations in the control vector $u_c = \begin{pmatrix} \ddot{\ell} & \ddot{\delta} \end{pmatrix}$. One may argue that such sudden control actions might not be properly approximated by the interpolating polynomial.
- It may also be of interest to define a range for ℓ so the length of the tether does not dramatically increase or decrease in case no target trajectory is provided with the aim of maximizing the tension.
- Analogously, some limits for the position of the center of mass shall be provided so that the solution is physical. It may happen that the solver finds an optimal trajectory at a negative height.

5 | Socio-Economic Impact

Airborne Wind Energy Systems can be regarded as a relatively, albeit not entirely, new way of energy extraction. Its renewable nature is in part responsible for its fast growth and development in the last few years. Recalling the numerous players introduced in section 1.2.4, it is possible to infer the size of the whole industry. There is already a lot of workforce involved in this sector and it is supposed to grow in the near future. Closely looking at the problem, one may realize all the required systems and technology are already developed, either coming from the kite-surf world or aviation. A proper merging and adaptation is then the only critical gap to success at a first glance.

Notwithstanding, there is still much more to be done before this gap can be bridged. As it will be discussed in the following section, there are various legal and financial aspects that need to evolve together with the technology. Up to now, none of the players have shown a reliable performance, rendering parallel works very helpful even for the cutting-edge, more mature companies. In this regard, the current project can be used to explore a different branch of flying devices, i.e. those without de-powering capabilities. The only application that comes to mind at first glance is cargo or vehicle traction, considering reel-in phase in a flaggered state a rather unreliable and unpredictable procedure. However, it is likely that a kitesurf-based system with angle of attack control loses this capacity in one way or another, e.g. an electronic device failure or tether breakage. In that particular situation this study may provide useful results and conclusions so to design an emergency protocol aimed at minimizing its associated damage.

Nowadays there is a huge amount of development and documentation on control design. Nevertheless, it often implies a previous formation on control theory and mathematics that some users cannot cope with. This does not necessarily imply they do not know how to implement a given control scheme but what is best to implement where. The problem of study might well fall under these characteristics since it based upon a highly non-linear model with modest control capabilities. The latter characteristics drove the path controller complexity from an initial velocity direction based PID control to a Non-linear Dynamic Inversion correction. Since none of them seemed to be valid even for a first approximation, a much more complex scheme needed to be developed. Therefore, this project can be referred to by users struggling to develop solutions for limited control capacity problems.

Table 5.1 Project Budget, detailed in Appendix B

CONCEPT	FIGURES
Research Scholarship Holder	
Salary:	1345.67 €/month
Average laboral days considering 10 days plus 4-week vacations:	19.241 days/month
Laboral day workhours:	8 hours/day
Total project duration, according to Bologna Process:	30 hours/ECTS × 12 ECTS
AMOUNT	**3147.19 €**
Doctor in Aerospace Engineering	
Salary:	1870.02 €/month
Participation in the project:	≈ 5 hours/week
Considering the working conditions stated above:	· 19.241 days/month · 8 hours/day · 9 weeks project duration
AMOUNT	**546.69 €**
Equipment Depreciation	
Laptop cost:	1087.75 €
Typical laptop lifespan:	8 years
Considering linear depreciation and professional use only:	· 19.241 days/month · 8 hours/day · 400 hours project duration
AMOUNT	**23.45 €**
Computational Costs	
Laptop's average power:	107.3 W
Red Eléctrica de España energy price by 09/09/2018:	0.14457 €/kWh
Estimated computational time:	400 hours
AMOUNT	**6.21 €**
Software License	**1200 €**
TOTAL	**4923.54 €**

6 | Regulatory Framework

In order to consider the legal environment of Airborne Wind Energy, it is necessary to assess the current stage of the technology and its market niche. Udo Zillmann and Sebastian Hach in chapter 7 of [1] performed an analysis back in 2013, but the scenario has not significantly changed as stated by Kristian Petric in [20]. They both claim AWE is among the phases of Applied Research and Technological Demonstration according to the scheme of the typical life-cycle of a venture. Both Zillmann, U. and Petric, K. are members of Airborne Wind Europe, which is essentially an association of AWE companies aimed at dealing with legal and financial issues. Airborne Wind Europe's activities, among others, comprise continuous communication with the European Commission and Member States to inform the sector about the different *push-policies*[1] that are currently or will shortly be carried out. It is also in charge of publishing some recommendations as outcomes of economic and sector based studies (including interviews and consultations) that individual companies may not be able to perform by their own. There are numerous programmes from which the AWE Industry can benefit, either in the United States or the European Union. In the latter case, the novel off-shore wind farms (which in fact turned out to be a successful and efficient venture) entailed solid and up-to-date foundations, indeed some of the policies launched for their development also apply to AWE.

Nevertheless, due to the lack of technology demonstration, Regulating Authorities have not yet created a specific regulatory framework in terms of health and safety standards or even airspace management. In this regard, Airborne Wind Europe as a representative of the whole industry is gathering information and requesting movements from the regulators side. Volkan Salma et al. in chapter 29 of [1] claim that Ampyx Power is seeking the certification of a utility scale rigid glider through conversations with EASA. Ampyx Power company itself references two EASA public documents[2] in their official web page and suggests there are movements towards the creation of a regulatory framework for unmanned tethered vehicles. Thereafter, it is possible to arrive at two different EASA published documents, one in the form of a Notice of Proposed Amendment[3] and another

[1] *Push-policies* are released by governments and regulators in order to promote the growth of a certain sector or technology. This support usually comes in the form of grants, public equity, low interest loans or tax credits.

[2] https://www.ampyxpower.com/safety-certification

[3] https://www.easa.europa.eu/document-library/notices-of-proposed-amendments/npa-2014-09

one in the form of a Concept of Operations[4]. The latter document gives an overall view on the different categories of drones, depending on their use and specifications. Due to the commercial purposes of Airborne Wind Energy Systems, it is straightforward to notice they may well lie under the "certified" category. More importantly, given an AWES that operate at a height below 500 ft above ground level, GM1 SERA.3138(a) can apply to it, so the operator shall comply with the applicable requirements in the Annexes to Regulation (EC) No 216/2008[5]. In case a tethered aircraft exceeds the aforementioned height (500 ft), the operator shall hold a valid certificate for handling Remote Piloted Aircraft Systems (RPAS) and shall be able to guarantee an adequate level of safety during the whole operation.

[4] https://www.easa.europa.eu/document-library/general-publications/concept-operations-drones

[5] https://eur-lex.europa.eu/legal-content/EN/TXT/?uri=CELEX:02008R0216-20160126

Bibliography

[1] U. Ahrens, M. Diehl, and R. Schmehl. *Airborne Wind Energy*. Green Energy and Technology. Springer Berlin Heidelberg, 2013.

[2] Juan Carlos Albahaca. Analytical and numerical study of the poincaré map with applications on the computation of periodic orbits. 2015.

[3] Joel Andersson. *A General-Purpose Software Framework for Dynamic Optimization*. PhD thesis, Arenberg Doctoral School, KU Leuven, Department of Electrical Engineering (ESAT/SCD) and Optimization in Engineering Center, Kasteelpark Arenberg 10, 3001-Heverlee, Belgium, October 2013.

[4] Philip Bechtle, Mark Schelbergen, Roland Schmehl, Udo Zillmann, and Simon Watson. Airborne wind energy resource analysis. *arXiv preprint arXiv:1808.07718*, 2018.

[5] Guillermo Escribano Blázquez. Review on airborne wind energy systems. 2018.

[6] Long-Yi Chang and Hung-Cheng Chen. Linearization and input-output decoupling for nonlinear control of proton exchange membrane fuel cells. *Energies*, 7(2):591–606, 2014.

[7] Nathan L. Chang, Anita Wing Yi Ho-Baillie, Doojin Vak, Mei Gao, Martin A. Green, and Renate J. Egan. Manufacturing cost and market potential analysis of demonstrated roll-to-roll perovskite photovoltaic cell processes. *Solar Energy Materials and Solar Cells*, 174:314 – 324, 2018.

[8] Antonello Cherubini, Andrea Papini, Rocco Vertechy, and Marco Fontana. Airborne wind energy systems: A review of the technologies. *Renewable and Sustainable Energy Reviews*, 51:1461 – 1476, 2015.

[9] B. Etkin. *Dynamics of flight: stability and control*. John Wiley & Sons Australia, Limited, 1982.

[10] Uwe Fechner and Roland Schmehl. Downscaling of airborne wind energy systems. *Journal of Physics: Conference Series*, 753(10):102002, 2016.

[11] Uwe Fechner and Roland Schmehl. Flight path control of kite power systems in a turbulent wind environment. 07 2016.

[12] Aysun Güner and Salih Yalçınbaş. Legendre collocation method for solving nonlinear differential equations. *Mathematical and Computational Applications*, 18(3):521–530, 2013.

[13] L.N. Hand and J.D. Finch. Analytical mechanics. 1998.

[14] T. Harmark. Notes on lie derivatives and killing vector fields. 2008. http://www.nbi.dk/~harmark/Killingvectors.pdf.

[15] C. Jehle. Automatic flight control of tethered kites for power generation. 2012.

[16] Costas Kravaris and Masoud Soroush. Synthesis of multivariable nonlinear controllers by input/output linearization. *AIChE Journal*, 36(2):249–264, 1990.

[17] Miles L. Loyd. Crosswind kite power. 4:106–111, 06 1980.

[18] Lara, M. and Peláez, J. On the numerical continuation of periodic orbits - an intrinsic, 3-dimensional, differential, predictor-corrector algorithm. *A&A*, 389(2):692–701, 2002.

[19] Alejandro Pastor-Rodríguez, Gonzalo Sanchez-Arriaga, and Manuel Sanjurjo Rivo. Modeling and stability analysis of tethered kites at high altitudes. *Journal of Guidance, Control, and Dynamics*, 40:1892–1901, 08 2017.

[20] K Petrick. Policies for airborne wind energy – preparing the grounds for awe-specific incentive schemes (scoping study. *Airborne Wind Europe, Brussels*, 2018.

[21] A.J. Otero Ramírez. Control system and hardware-related elements applied to flight testing of airborne wind energy systems. 2018.

[22] G Sánchez-Arriaga, A Pastor-Rodríguez, R Borobia-Moreno, and R Schmehl. A constraint-free flight simulator package for airborne wind energy systems. 1037(6):062018, 2018.

[23] D.E. Seborg, D.A. Mellichamp, T.F. Edgar, and F.J. Doyle. *Process Dynamics and Control*. John Wiley & Sons, 2010.

[24] Dian J. Seidel, Chi O. Ao, and Kun Li. Estimating climatological planetary boundary layer heights from radiosonde observations: Comparison of methods and uncertainty analysis. *Journal of Geophysical Research: Atmospheres*, 115(D16).

[25] Manuel Soler, Daniel Expósito, and G. Sánchez-Arriaga. Determination of optimal control laws in airborne wind energy scenarios with a self-consistent kite dynamics model. *Book of abstract of AWEC*, page 120, 2017.

[26] G. Sánchez-Arriaga, M. García-Villalba, and R. Schmehl. Modeling and dynamics of a two-line kite. *Applied Mathematical Modeling*, 47:473 – 486, 2017.

[27] Andreas Wächter and Lorenz T. Biegler. On the implementation of an interior-point filter line-search algorithm for large-scale nonlinear programming. *Mathematical Programming*, 106(1):25–57, Mar 2006.

[28] Kewei Xia and Wei Huo. Robust adaptive backstepping neural networks control for spacecraft rendezvous and docking with uncertainties. *Nonlinear Dynamics*, 84(3):1683–1695, May 2016.

[29] S. Zhang and W.-q. Qian. Dynamic backstepping control for pure-feedback nonlinear systems. *ArXiv e-prints*, jun 2017.

APPENDICES

A | Simulink Implementation and NDI Controller

A.1 Simulink Model

Hereafter, the implementation of a controller in SIMULINK MATLAB add-on is presented. The selection of such software is mainly driven by its user friendly interface, that allows a visual separation of the different systems. In fact, SIMULINK is capable of compiling the model in C or C++ languages, therefore aiding the developer in the early stages of hardware implementation. Figure **??** depicts a block diagram of the KiteAcrobat model in SIMULINK workspace. Its functionality is exactly equal to the MATLAB model itself, meaning that it propagates the dynamics of the system given a set of initial conditions and a control law. The circular block on the left displays and provides the current simulation time, which is input to the controller and equations of motion blocks. The control law in this simple model is merely a function of time so this is still open-loop control, thus its validation simply consists in comparing SIMULINK and MATLAB model results. As mentioned in section 3.3 the initial conditions inserted in the periodic orbit solver presented in section 3.2 were determined by varying the values inside the "ICs" block and integrating the Initial Value Problem for a considerable amount of time - until convergence seems to occur.

A.2 NDI velocity vector based controller

This section is devoted to the discussion of the SIMULINK model illustrated in figure A.2. It has been previously mentioned that the controls must be bounded at least up to the second derivative. In this regard, the equations of motion of the system were modified to inherit the controls and their first derivative, rendering the second derivative the "actual" controls[1]. Now the selection of the initial conditions for the new variables introduced in the state vector is crucial since they must be consistent with the attitude inferred from the other variables. Keeping this in mind, the open-loop control law albeit introducing an initial error resulting from the difference between the

[1] Hence the state vector u is rewritten as extended state vector u_{amp} and $u_c = \begin{pmatrix} \ddot{\ell} & \ddot{\delta} \end{pmatrix}$

target and the base trajectory, turns out to be the best option. It can be assumed that such perturbation should be easily overcome by the controller, especially considering the small differences of the first approximation: see figure 4.1.

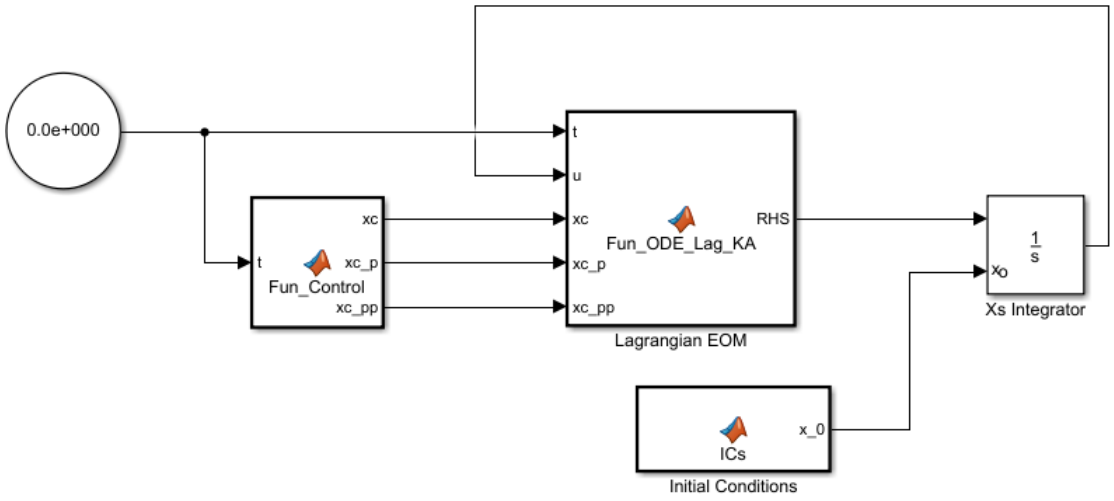

Figure A.1: KiteAcrobat Model implemented on SIMULINK software

The reader should note this specific controller was the last version considered before posing the optimal control problem. Some of the different intermediate versions showing the development of the control scheme are listed below:

- PD controller based on the error between the current position and velocity direction of the center of mass with respect to the closest point of the trajectory, only applying to $\ddot{\delta}$. Sign convention is given by the difference in the z-coordinate, if the target trajectory is at higher altitude a negative control action is performed.
- The next version also considers a PD controller but in this case it is merely based on the velocity direction. The angle between the current velocity direction and the target one is now considered the velocity error. In the case of the position error, some way point within the target trajectory ($\mathbf{r}^*$) ahead of the closest one to $\mathbf{x_{cg}}$ is defined so the vector difference $\mathbf{r}^* - \mathbf{x_{cg}}$ is the direction to be compared with $\dot{\mathbf{x}}_{\mathbf{cg}}$. Angle sign convention is given by the z_E axis depicted in figure 2.1, positive counterclockwise.
- The final version introduced input-output linearization in order to account for non-linearities. The reader should note the system does not respond to controls in a linear way, so the same error may require different control actions depending on the attitude of the kite. By means of the *Lie Derivative* it is possible to perform a state transformation to a linearizing state [6][2], thus being able to apply the previously developed PD considering some non-linear dynamics.

[2] More on this can be found in TU Delft lecture notes http://www.aerostudents.com/courses/advanced-flight-control/nonlinearDynamicInversion.pdf

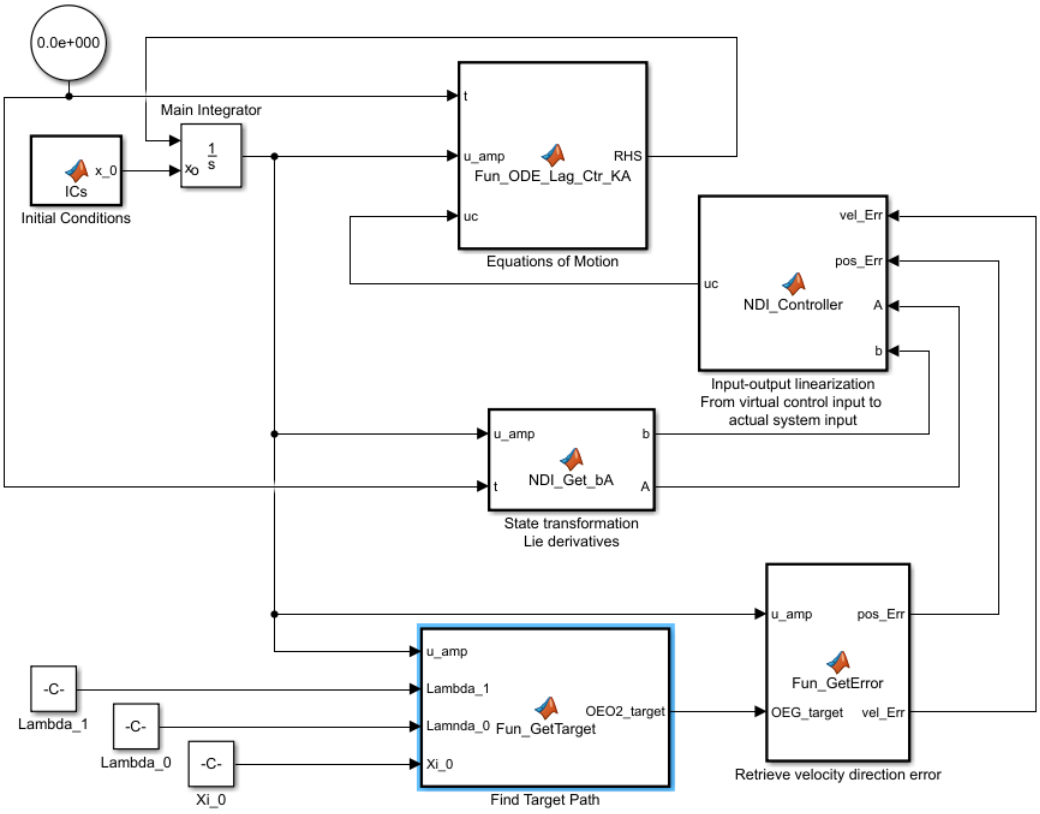

Figure A.2: Velocity direction-based NDI controller

Hereafter, a thorough discussion on the implementation of the NDI technique summarized in section 1.3.3 to the current two-line kite model is presented. The very first task consists in identifying which are the inputs and outputs of the system from the controller perspective. The control input has been selected as the second derivative of the former control variable $\ddot{\delta}$, while the output of the system is the position of the center of mass of the kite. Note that despite the use of a velocity direction based controller, the ultimate output is $\mathbf{x_{cg}}$ since the target trajectory is based upon this state. By analyzing the equations of motion it is possible to observe a linear relation between the acceleration of the center of gravity and the control input, yielding $k = 2$ in equation 1.4. As it was inferred in section 1.3.3 there will be some internal dynamics that will not be observed by the system, as a result of the relative degree of the input-output linearization k_{tot} being clearly lower than the order of the system (12)[3]. Nevertheless it is of interest to perform such input-output linearization and check *a posteriori* whether these dynamics are stable or not, mainly due to their non-linearity rendering the stability analysis a rather complex procedure. Let's consider the system:

$$\dot{\mathbf{x}} = \mathbf{f}(\mathbf{x}) + \mathbf{g}(\mathbf{x})\mathbf{u} \tag{A.1}$$

[3] In this case all the variables included in the output vector have the same individual relative degree, resulting in a total relative degree $k_{tot} = 6$.

$$\mathbf{y} = \mathbf{h}(\mathbf{x}) \tag{A.2}$$

Where $\mathbf{x}$ represents the state vector of size m, $\mathbf{u}$ represents the control vector of size n and $\mathbf{y}$ is the output of the system of size p. Let the *Lie Derivative* of the scalar function h with respect to the function $\mathbf{f}$ be:

$$L_{\mathbf{f}}h(\mathbf{x}) = \nabla h(\mathbf{x})\mathbf{f}(\mathbf{x}) = \sum_{i=1}^{m} \frac{\partial h(\mathbf{x})}{\partial x_i} f_i(\mathbf{x}) \tag{A.3a}$$

$$L_{\mathbf{f}}^{k}h(\mathbf{x}) = L_{\mathbf{f}}h(\mathbf{x}) \left(L_{\mathbf{f}}^{k-1}h(\mathbf{x})\right) \tag{A.3b}$$

The k-th derivative of the output can be written in terms of the input variables by means of *Lie Derivatives*[4]. A good introduction to the definition of such derivatives can be found in [14], together with some interesting applications. One can think of the *Lie Derivative* of a function f along a vector field g, $L_g f$, as the change in f in the direction of the flow of g, understanding the flow as a differentiable function that is always tangent to the vector field. In the end, the controller scheme in the form of 1.4 can be written as:

$$\bar{\bar{A}}(\mathbf{x}) = \begin{bmatrix} \sum_{j=1}^{m} \frac{\partial\left(\sum_{i=1}^{m} \frac{\partial h_1(\mathbf{x})}{\partial x_i} f_i(\mathbf{x})\right)}{\partial x_j} g_{j,1}(\mathbf{x}) & \dots & \sum_{j=1}^{m} \frac{\partial\left(\sum_{i=1}^{m} \frac{\partial h_1(\mathbf{x})}{\partial x_i} f_i(\mathbf{x})\right)}{\partial x_j} g_{j,n}(\mathbf{x}) \\ \vdots & \ddots & \vdots \\ \sum_{j=1}^{m} \frac{\partial\left(\sum_{i=1}^{m} \frac{\partial h_p(\mathbf{x})}{\partial x_i} f_i(\mathbf{x})\right)}{\partial x_j} g_{j,1}(\mathbf{x}) & \dots & \sum_{j=1}^{m} \frac{\partial\left(\sum_{i=1}^{m} \frac{\partial h_p(\mathbf{x})}{\partial x_i} f_i(\mathbf{x})\right)}{\partial x_j} g_{j,n}(\mathbf{x}) \end{bmatrix}$$

$$\mathbf{b}(\mathbf{x}) = \begin{bmatrix} \sum_{j=1}^{m} \frac{\partial\left(\sum_{i=1}^{m} \frac{\partial h_1(\mathbf{x})}{\partial x_i} f_i(\mathbf{x})\right)}{\partial x_j} f_j(\mathbf{x}) \\ \vdots \\ \sum_{j=1}^{m} \frac{\partial\left(\sum_{i=1}^{m} \frac{\partial h_p(\mathbf{x})}{\partial x_i} f_i(\mathbf{x})\right)}{\partial x_j} f_j(\mathbf{x}) \end{bmatrix} \qquad \mathbf{v} = -\mathbf{K}_0\varepsilon_0 - \mathbf{K}_1\varepsilon_1$$

$$\mathbf{u} = \bar{\bar{A}}^{-1}(\mathbf{x}) \left(\mathbf{v} - \mathbf{b}(\mathbf{x})\right)$$

Where for the current application:

- The order of the system is $m = 12$ and the sizes of the control and output vectors are $n = 2$ and $p = 3$ respectively.
- The individual relative degrees (all equal to two) have been substituted, as well as the *Lie Derivatives*.
- Virtual control input $\mathbf{v}$ is clearly a vector, whereas the position and velocity errors are scalars (recall they are the difference in velocity direction). Therefore $\mathbf{K}_0$ and $\mathbf{K}_1$ are two vectors of constants.

[4] That derivation is outside of the scope of the current paper, mainly considering a Non-Linear Dynamic Inversion controller is not the main outcome of the project. Nevertheless [16] contains an in-depth explanation on this.

B | Project Budget Breakdown

Due to the "Research & Development" nature of the project, the proposed budget is based on a general academic environment. Both scholarship and former doctor's remunerations were retrieved from the salaries published by Universidad Carlos III de Madrid[1]. Staff is supposed to have a usual 8-hour workday and 10 days plus 4 weeks yearly holidays so that:

$$5\,\frac{workdays}{week}\times\frac{365.244}{7\times 12}\frac{weeks}{month}-\frac{10\,\frac{free\,days}{year}+4\times 5\,\frac{vacation\,days}{year}}{12\,\frac{months}{year}}=19.24061\,\frac{days}{month}$$

The total assumed hours correspond to those stated in Bologna Process, taking 30 hours as reference value for 1 ECTS credit.

$$Project\ Duration: 30\,\frac{hours}{ECTS}\times 12\,ECTS=360\,hours$$

Finally leading to the scholarship holder's expenditure:

$$\frac{1345.67\,\frac{€}{month}}{19.241\,\frac{days}{month}\times 8\,\frac{hours}{day}}\times 360\,hours=3147.193\,€$$

Considering the extension in time of the project as a result of part-time involvement, the weekly participation of the supervisor was increased to 5 hours per week. This constitutes 1/8 of his total workforce for 9 weeks:

$$5\,\frac{hours}{week}\times\frac{360\,hours}{8\,\frac{hours}{day}\times 5\,\frac{days}{week}}=5\,\frac{hours}{week}\times 9\,weeks=45\,hours \tag{B.1}$$

Therefore, the aerospace engineering doctor's fees would read:

$$\frac{1870.02\,\frac{€}{month}}{19.241\,\frac{days}{month}\times 8\,\frac{hours}{day}}\times 45\,hours=546.690\,€$$

Let's consider the equipment depreciation. Equipment overall costs are summarized below:

[1] https://www.uc3m.es/ss/Satellite/UC3MInstitucional/es/TextoMixta/1371208973960/Retribuciones

Table B.1 Equipment Costs Breakdown

Item	Description	Amount
Acer Aspire V3-772G[2]	17.3-inch Screen Laptop Intel core i7-4702MQ 8 GB DDR3L RAM 1 TB HDD Drive	900 €
Kingston KVR16LS11/8[3]	1× 8 GB DDR3L compatible RAM socket	65 €
Crucial MX500[4]	500 GB 2.5-inch SSD Drive	122.75 €

The laptop was purchased on 31/03/2014, while the rest of components were acquired by 21/03/2018. Assuming linear weekly-based depreciation and a typical lifespan of 8 years for a 2014 laptop:

$$\frac{1087.75\,\frac{€}{month}}{365.2422\,\frac{days}{year}\times 8\,years \div 7\,\frac{days}{week}}\times 9\,weeks = 23.453\,€$$

According to Sebastian Jentsch's review for Notebookcheck[5], the measured power consumption may be in the range $85.6 - 129$ Watts. PVPC[6] price given by the Spanish National Government is a good indicative of the energy price. Due to the diverse simulations the estimated computational time is slightly higher than the actual project duration, around 400 hours.

$$\frac{85.6+129}{2}\times 10^{-3}\,kW \times 0.14457\frac{€}{kWh}\times 400\,hours = 6.205\,€$$

The software licenses limit to an annual license for MATLAB and SIMULINK software[7]. Note Python is not an good alternative since SIMULINK add-on was used to implement an alternative controller, even though it did not perform as expected.

[2] https://www.acer.com/ac/en/US/content/support-product/4732?b=1
[3] https://www.amazon.es/dp/B00CQ35HBQ/ref=pe_3310721_189395781_TE_dp_1
[4] https://www.amazon.es/dp/B0784SLQM6/ref=pe_3310721_189395781_TE_dp_2
[5] https://www.notebookcheck.net/Review-Acer-Aspire-V3-772G-747A321-Notebook.93916.0.html
[6] https://www.esios.ree.es/es/pvpc as of 09/09/2018.
[7] https://es.mathworks.com/pricing-licensing.html?prodcode=SL&intendeduse=undefined